Defining how Pak1 regulates cell polarity and cell division in fission yeast

Joseph O. Magliozzi,[1] Jack Sears,[1,2] Marielle Brady,[1] Hannah E. Opalko,[1] Arminja N. Kettenbach,[1,2] and James B. Moseley[1]

[1] Department of Biochemistry and Cell Biology, The Geisel School of Medicine at Dartmouth, Hanover, NH 03755, USA

[2] Norris Cotton Cancer Center, The Geisel School of Medicine at Dartmouth, Lebanon, NH 03756, USA

* Corresponding author
james.b.moseley@dartmouth.edu

Number of characters: 38,893

Running title: Pak1 regulates cell division

SUMMARY

Magliozzi et al. show that fission yeast Pak1 regulates multiple events during cell division. Through a phosphoproteomic screen and subsequent mutant analysis, their work uncovers direct targets and mechanisms for Pak1 activity during cell growth and division.

ABSTRACT

Protein kinases direct polarized growth by regulating the cytoskeleton in time and space, and could play similar roles in cell division. We found that the Cdc42-activated polarity kinase Pak1 colocalizes with the assembling cytokinetic ring and remains at the division site during septation. Mutations in *pak1* led to defects in cytokinetic ring assembly and cell separation. Through a phosphoproteomic screen, we identified novel Pak1 targets that function in polarized growth, cytokinesis, and septation. For cytokinesis, we found that Pak1 regulates the localization of its substrates Mid1 and Cdc15 to the cytokinetic ring. For cell separation, Pak1 phosphorylates the RNA-binding protein Sts5 to prevent its assembly into granules. These results show that Pak1 acts directly on components of the cytokinetic ring, and unexpectedly promotes the later stages of cell division by inhibiting the assembly of ribonucleoprotein granules. More broadly, our work reveals that cell polarity signaling proteins coordinate diverse events to promote cell division at the end of the cell cycle.

INTRODUCTION

The processes of cell polarization and cytokinesis share a requirement for the assembly of actin filaments into higher-order structures that are physically linked to the cell cortex. For example, polarized actin cables, actomyosin stress fibers, and dendritic actin networks are central to the establishment, maintenance, and regulation of cell polarity in both yeast and metazoan cells (Tojkander et al., 2012; Chiou et al., 2017; Omotade et al., 2017). The architecture of these actin structures is controlled by cell polarity signaling proteins, which relay spatial landmarks in the cell to the cytoskeleton. Polarity signaling proteins also have the potential to function in other cellular processes that require manipulation of the cytoskeleton, such as in cytokinesis. Yeast and metazoan cells dramatically reorganize the actomyosin cytoskeleton into a contractile actomyosin ring (CAR) to promote the process of cytokinesis. Past work has shown that cortical cell polarity proteins indirectly regulate cytokinesis by positioning the mitotic spindle, but few studies have considered that cell polarity proteins might act directly on the CAR. Decades of elegant work demonstrated that the metazoan spindle positions the assembly of the CAR (Rappaport et al., 2009). Both the spindle midzone and astral microtubules provide spatial signals for cytokinesis (Bringmann and Hyman, 2005). Cortical cell polarity proteins anchor dynein motors at cell ends to pull astral microtubules, thereby positioning the spindle as a spatial cue for CAR assembly (Siller and Doe, 2009; Kotak and Gönczy, 2013). Cell polarity proteins act indirectly through the spindle in this model, but there are hints of more direct links between cell polarity proteins and the CAR. For example, cell polarity factors position the CAR in fly neuroblasts that are induced into cytokinesis in the absence of a mitotic spindle (Cabernard et al., 2010). Further, cortical cell polarity factors contribute to the robustness of cytokinesis in dividing *C. elegans* embryos (Davies et al., 2016; Jordan et al., 2016). In this study, we investigated the possibility of a direct role for polarity signaling factors during cytokinesis of fission yeast cells.

Fission yeast has served as a long-standing model system for studies on both cell polarity and cytokinesis. These rod-shaped eukaryotic cells grow in a highly polarized manner at their tips during interphase (Fantes and Nurse, 1977). Genetic screens have identified conserved polarity factors essential for this shape and growth pattern (Hayles and Nurse, 2001). An early screen isolated a class of round (or “orb”) mutants that were enriched for protein kinases, showing the importance of signaling in cell polarity (Snell and Nurse, 1994; Verde et al., 1995). This group includes Pak1, also called Orb2 or Shk1, which is a member of the PAK (p21-activated kinase) family of protein kinases (Marcus et al., 1995). PAK kinases are auto-inhibited until activation by binding to the GTP-bound form of the GTPase Cdc42, a global regulator of cell polarity (Bokoch, 2003). Active PAK kinases then organize and orient the cytoskeleton by phosphorylating downstream substrates. In fission yeast, Pak1 has been shown to phosphorylate several proteins *in vitro* (Yang et al., 1999; Endo et al., 2003; Kim et al., 2003; Yang et al., 2003; Loo and Balasubramanian, 2008), but we do not have a comprehensive understanding of *in vivo* Pak1 targets and their functional connections to cell polarity and/or cell division.

Beyond the *orb* screen that identified Pak1, additional studies identified more conserved protein kinases involved in cell polarity, including Pom1/DYRK and Kin1/MARK (Levin and Bishop, 1990; Bähler and Pringle, 1998). Together, these kinases and their underlying signaling pathways coordinate the events of polarized growth including cytoskeletal reorganization, cell wall remodeling, and membrane expansion (Sawin and Nurse, 1999; Drewes and Nurse, 2003; La Carbona et al., 2004; Bhatia et al., 2014; Rincon et al., 2014).

In fission yeast cells, polarized growth ceases as cells enter into mitosis and divide. At this stage, much of the cytoskeletal machinery that had powered polarized growth during interphase shifts to the cell middle to form the CAR through a tightly regulated process. Fission yeast has served as a strong model system for studying cytokinesis due to the highly

reproducible series of events leading to CAR assembly and constriction. Many of the proteins that participate in these events have been identified through decades of genetic screens and subsequent characterization (Chang et al., 1996; Wu et al., 2006; Pollard and Wu, 2010). Fission yeast cytokinesis occurs in four steps powered by the collective action of these proteins. First, a subset of cytokinesis proteins is recruited to 50-75 cortical spots called nodes, which are positioned in the cell middle (Chang et al., 1996; Sohrmann et al., 1996; Wu et al., 2006). The anillin-related protein Mid1 serves as the primary anchor to position cytokinetic nodes in the cell middle (Sohrmann et al., 1996; Paoletti and Chang, 2000; Celton-Morizur et al., 2006; Padte et al., 2006; Almonacid et al., 2009; Almonacid et al., 2011). The second step is CAR assembly, when cytokinetic nodes coalesce into an intact ring through actin-myosin based interactions (Wu et al., 2006; Vavylonis et al., 2008). The third step is CAR maturation, when additional cytokinesis proteins are recruited to the intact ring (Wu et al., 2003; Wu et al., 2006; Pollard and Wu, 2010). The fourth step is ring constriction, when the CAR constricts through the combined forces of actin-myosin and cell wall deposition (Liu et al., 1999; Sipiczki and Bozsik, 2000; Liu et al., 2002). During ring constriction, Mid1/anillin leaves the CAR and the F-BAR protein Cdc15 acts as a major anchor to scaffold multiple cytokinesis proteins with the ingressing membrane (Paoletti and Chang, 2000; Roberts-Galbraith et al., 2010; Martín-García et al., 2014; Ren et al., 2015; McDonald et al., 2017; Willet et al., 2019). This final step is coordinated with cell wall synthesis in the process of septation, which ultimately promotes separation of the two daughter cells (Jochovà et al., 1991; Proctor et al., 2012).

We recently identified a direct connection and functional role for the cell polarity kinases Pom1 and Kin1 in cytokinesis. Large-scale phosphoproteomic screens revealed that Kin1 and Pom1 phosphorylate multiple cytokinesis proteins, including several shared substrates (Kettenbach et al., 2015; Lee et al., 2018). Both *in vitro* and in cells, Kin1 and Pom1 phosphorylated largely non-overlapping residues on these shared substrates (Lee et al., 2018). Simultaneous inhibition of both kinases led to cytokinesis defects, including “unspooling” of the CAR during constriction (Lee et al., 2018). These results led us to hypothesize that additional cell polarity kinases might directly regulate cytokinesis proteins to promote cell division. Here, we performed a visual screen for cell polarity kinases that localize to the site of cytokinesis, and found a new role for Pak1 in CAR assembly and cell separation. Through large-scale phosphoproteomics, we have identified and characterized novel Pak1 substrates that regulate cell polarity, cytokinesis, and septation. Our study reveals mechanisms for how this conserved kinase controls diverse events in cell growth and division, and provides additional support for the role of cell polarity signaling in cytokinesis.

RESULTS

Cdc42-Pak1 localizes to the assembling CAR

To identify cell polarity kinases that might function in cytokinesis and cell division, we monitored the localization of seven mEGFP-tagged kinases during specific cell cycle stages using fluorescence microscopy. Each strain also expressed the myosin light chain Rlc1-mRuby2 to mark the CAR and Sad1-mCherry to mark the spindle-pole body (SPB), which allowed us to categorize kinase localization during defined stages of cell division (Fig. 1A). Six of the kinases were recruited to the cell middle late in the division process, after CAR assembly and during constriction. In contrast, Pak1 appeared at the division site earlier than other cell polarity kinases. Pak1 localized to the cell middle shortly after SPB splitting, when CAR node precursors were still coalescing into a ring.

Pak1 is a member of the PAK (p21-activated protein kinase) family, and has also been called Orb2 and Shk1 (Marcus et al., 1995; Verde et al., 1995). Based on its appearance at the division site during G2/M, we investigated Pak1 localization more closely. During interphase, Pak1 oscillated between the two cell ends in a pattern similar to that observed for the activated form of its upstream regulator Cdc42 (Figs. S1A-B; Das et al., 2012). At mitotic entry, Pak1 appeared in the cell middle and then in an intact ring (Figs. 1A, S1A). During CAR constriction and septation, Pak1 localized to two non-constricting rings adjacent to the CAR (Figs. 1A, S1A). We examined Pak1 localization during CAR assembly more closely using Airyscan confocal microscopy. Pak1 colocalized with CAR marker Rlc1 during ring assembly, but we also observed Pak1 signal at the division site that did not overlap with Rlc1. Interestingly, Pak1 appeared to form a connecting strand that linked two loose ends of the CAR in the final stages of assembly (Fig. 1B). These results suggest that Pak1 might function during multiple stages of cell division including CAR assembly and septation.

Pak1 function at the assembling CAR would likely require the presence of activated Cdc42, which binds to and activates Pak1. Cdc42 activity is downregulated during cytokinesis in budding yeast (Atkins et al., 2013), but Cdc42 activity during fission yeast CAR assembly has been unclear. Using the well-established Cdc42 biosensor CRIB-3xGFP (Tatebe et al., 2008), we found that active GTP-Cdc42 localized to the cell middle and assembling CAR similar to Pak1 (Fig. 1C, see also Fig. S1A). Both active Cdc42 and Pak1 localized to the cell middle during the assembly and maturation phases on cytokinesis (Fig. 1C). We conclude that active Cdc42 and Pak1 enrich at the assembling CAR and might contribute to the early stages of cytokinesis, unlike other cell polarity kinases that reach the cell middle only at the later stages of cell division.

Pak1 promotes CAR assembly, cytokinesis, and cell separation

Based on these localization results, we next tested if Pak1 functions in assembly of the CAR. *pak1* is an essential gene, so we used two different mutant alleles: analog-sensitive *pak1-as* (M460A) and temperature-sensitive *orb2-34* (a mutant allele of *pak1*). Both mutants exhibit partial loss-of-function phenotypes including increased cell width under permissive conditions, consistent with severely reduced kinase activity *in vitro* (Fig. S2A-B; Loo and Balasubramanian, 2008; Das et al., 2012). We measured the time between SPB splitting and complete CAR assembly (Fig. S2C), and found that both *pak1* mutants took longer to assemble the CAR than wild-type cells (Fig. 2A). CAR assembly was slowed even further by adding 3-Brb-PP1 inhibitor to *pak1-as* cells, which inhibits residual kinase activity in this mutant (Fig. S2D). In these mutants, longer CAR assembly was coupled with a shorter CAR maturation phase between assembly and constriction (Fig. S2E). Subsequent CAR constriction occurred with similar timing in the mutant and wild-type cells (Fig. S2E). Thus, Pak1 localizes to the assembling CAR and is required for efficient CAR assembly.

Analysis of synthetic genetic interactions provided additional support for the role of Pak1 in cytokinesis. We combined the *orb2-34* allele with *mid1-366* and *rng2-D5* temperature-sensitive mutants. Both Mid1/anillin and Rng2/IQGAP localize to cytokinesis nodes as well as the CAR and are critical for proper CAR formation (Eng et al., 1998; Wu et al., 2006, Laporte et al., 2011; Padmanabhan et al., 2011). We observed synthetic growth defects for both *orb2-34 mid1-366* and *orb2-34 rng2-D5* double mutants (Fig. 2B). Visual inspection of these cells revealed severe cytokinesis defects including misplaced, multiple, and/or disorganized division planes (Fig. 2C-E). We considered the possibility that these defects might be due to increased cell width in *orb2-34* mutants, as opposed to a more direct role in cytokinesis. To control for this possibility, we combined *mid1-366* and *rng2-D5* with *rga4*Δ, which exhibits increased cell width like *orb2-34* (Das et al., 2007). However, no synthetic defects were observed with *rga4*Δ (Fig. S2F), indicating that *orb2-34* genetic interactions likely reflect a role for Pak1 in CAR assembly.

In addition to cytokinesis, we observed a striking cell separation defect upon inhibition of Pak1 kinase activity. The septation index of *pak1-as* cells treated with 3-BrB-PP1 was more than double wild-type cells or uninhibited *pak1-as* cells (Fig. 3A-B). This result indicates that low levels of Pak1 activity are sufficient to promote cell separation, but complete inhibition of kinase activity prevents activities required for separation. Consistent with this possibility, we did not detect increased septation index for *orb2-34* cells (Fig. S2G), which have reduced but not abolished kinase activity like uninhibited *pak1-as*. Taken together, our results show that Pak1 localizes to the site of cell division and promotes key events in cytokinesis and cell separation.

pak1 mutant defects are independent of Rlc1 phosphorylation

What proteins does Pak1 phosphorylate to promote cell division? One candidate substrate for this function is Rlc1, the regulatory light chain of myosin II. Past work has shown that Pak1 phosphorylates Rlc1 at residues S35 and/or S36 (Loo and Balasubramanian, 2008). We performed *in vitro* kinase assays with purified proteins and found that Pak1 phosphorylates Rlc1-S36A, but not Rlc1-S35A or Rlc1-S35A,S36A (Fig. 4A; Fig. S3A). Therefore, Pak1 directly phosphorylates Rlc1 on residue S35. We next integrated non-phosphorylatable Rlc1 mutants into fission yeast cells. Each construct was tagged with mNeonGreen and expressed from the endogenous *rlc1* promoter. The non-phosphorylatable mutants did not exhibit defects in cell shape, CAR assembly, or septation (Fig. 4B-D). Moreover, these *rlc1* mutants did not have negative genetic interactions with *mid1-366* (Fig. 4E). We conclude that Pak1 phosphorylates Rlc1, but this substrate does not explain the role of Pak1 in CAR assembly and septation. Rather, these results suggest that additional cytokinesis proteins may be phosphorylated by Pak1 to promote cell division.

Large-scale phosphoproteomic screen reveals novel Pak1 substrates

To identify Pak1 substrates in cell division, we performed an unbiased phosphoproteomic screen. For this large-scale screen, we quantitatively compared the phosphoproteome before and after Pak1 inhibition using multiplexed tandem-mass-tag (TMT) labeling coupled with liquid chromatography and mass spectrometry. We tested 4 conditions: (1) *pak1-as* + methanol control, (2) *pak1-as* + 3-BrB-PP1, (3) wild-type + methanol control, and (4) wild-type + 3-BrB-PP1 (Fig. 5A). By using 11-plex TMT labeling, we directly compared the abundance of tryptic phospho-peptides from 11 samples: the first 3 conditions in triplicate and the final condition in duplicate. By including replicates, we could calculate statistical significance of phosphorylation site changes between conditions. In total, we identified 11,292 phosphopeptides, 8,641 phosphosites and 1,848 phosphoproteins (Table S2). *pak1-as* cells exhibit cell polarity and cytokinesis defects in the absence of inhibitor due to dramatically reduced kinase activity, so we expected to find cell polarity and cytokinesis substrates when comparing *pak1-as* versus wild-type, both lacking inhibitor. In this category, we identified 123 phosphopeptides reduced at least two-fold with a p-value of ≤ 0.05. This list included proteins that function in cell polarity (e.g. Scd1, Scd2, Tea3, and Rga4) and cytokinesis (e.g. Mid1, Cdc15, Cyk3, and Rng10) (Fig. 5B, Table S2). We reasoned that Pak1 substrates in septation may display even further reduced phosphorylation in the presence of 3-BrB-PP1, which triggers the cell septation defect in *pak1-as* cells. Two proteins with functional links to septation were found to have reduced phosphorylation in *pak1-as* cells and further reduction upon addition of 3-BrB-PP1 (Fig. 5C). These proteins, Sts5 and Etd1, represent candidate substrates for Pak1 function in septation (Fig. 5C). Below, we show that many of these proteins are direct substrates of Pak1, and reveal new regulatory mechanisms for how Pak1 promotes cell polarity, cytokinesis, and septation.

Pak1 phosphorylates cell polarity proteins

We performed *in vitro* kinase assays with purified proteins and γ-^{32}P-ATP to test if Pak1 directly phosphorylates the cell polarity proteins Scd1, Rga4, and Tea3. Scd1 is a Cdc42 guanine nucleotide exchange factor (GEF) known to complex with Pak1; Rga4 is a Cdc42 GTPase activating protein (GAP); and Tea3 is a scaffold protein for cell polarity proteins at cell ends (Chang et al., 1994; Arellano et al., 2002; Coll et al., 2003; Endo et al., 2003; Das et al., 2007; Tatebe et al., 2008; Geymonat et al., 2018). We purified full-length Tea3, and fragments of Scd1 and Rga4 containing residues phosphorylated in a Pak1-dependent manner in cells (Fig. S3A). All 3 cell polarity proteins were directly phosphorylated by Pak1 but not by kinase-dead Pak1(K415R) *in vitro*, confirming that they are Pak1 substrates (Fig. 6A).

Next, we used live-cell microscopy to test how Pak1 regulates these cell polarity substrates in cells. In wild-type cells, Scd1-mNG enriched at cell tips and in the nucleus during interphase, as previously shown (Hirota et al., 2003; Das et al., 2012). Nuclear enrichment of Scd1 was lost in *pak1-as* cells (Fig. 6B), meaning that Pak1 regulates nuclear localization of its substrate Scd1. Unlike Scd1, Tea3 localized exclusively at cell tips and was not impaired in *pak1-as* cells (Fig. 6C). Rga4 localized to cortical puncta that were excluded from cell tips, as previously shown (Das et al., 2007; Tatebe et al., 2008). Rga4-mNG puncta appeared denser and/or larger in *pak1-as* cells. Using quantitative Airyscan Super-Resolution microscopy, we measured a significant increase in Rga4 intensity per puncta for *pak1-as* cells compared the wild-type cells (Fig. 6D). This result indicates that Pak1 regulates the clustering of its substrate Rga4. Another cell polarity kinase, Pom1, prevents accumulation of Rga4 clusters at one of the cell tips (Tatebe et al., 2008). We combined analog-sensitive mutations in Pom1 and Pak1 to generate the strain *pom1-as pak1-as*, and then tested Rga4 localization upon inhibition of these two upstream regulatory kinases. Remarkably, Rga4 became enriched at both cell tips upon simultaneous inhibition of Pom1 and Pak1 (Fig. 6E). Thus, Pak1 regulates the clustering and tip exclusion of its substrate Rga4. These combined experiments reveal new substrates and regulatory mechanisms for how Pak1 promotes polarized growth. Further, these results demonstrate that our phosphoproteomic screen has identified *bona fide* substrates that act downstream of Pak1 in cells.

Pak1 phosphorylates cytokinesis proteins Mid1, Cdc15, and Cyk3

Our screen identified several potential cytokinesis-related substrates of Pak1. These targets included the anillin-like protein Mid1, which localizes to CAR node precursors and the mature CAR, and is required to position the CAR in the cell middle (Celton-Morizur et al., 2006; Padte et al., 2006; Almonacid et al., 2009; Almonacid et al., 2011; Chang et al., 1996; Paoletti and Change, 2000). The Mid1 N-terminus (Mid1-Nter, residues 1-506) localizes to nodes and the CAR, and is both necessary and sufficient for Mid1 function in cytokinesis (Celton-Morizur et al., 2004; Guzman-Vendrell et al., 2013). The Mid1 C-terminus contains a membrane-binding amphipathic helix that reinforces Mid1 localization (Celton-Morizur et al., 2004). We identified two Pak1-dependent phosphorylation sites at S328 and S331 in the N-terminus of Mid1 (Fig. 7A). We purified a Mid1 fragment spanning residues 300-450 and confirmed direct phosphorylation by Pak1 *in vitro* (Fig. 7B). Thus, Mid1 is a substrate of Pak1. We did not observe obvious defects in the localization of Mid1-mNG in *pak1-as* cells (Fig. S3B), so we focused on the Mid1-Nter construct that contains Pak1 sites. Consistent with past work, GFP-Mid1-Nter localized to cortical nodes in the cell middle and supported proper positioning of the cell division plane (Almonacid et al., 2009; Guzman-Vendrell et al., 2013). However, both the localization and function of Mid1-Nter were disrupted in *pak1-as* cells. GFP-Mid1-Nter still localized to the cell cortex in *pak1-as* cells, but not in nodes that concentrated in the cell middle (Fig. 7C). This mislocalization correlated with dramatic cytokinesis defects, as *GFP-mid1-Nter pak1-as* cells exhibited a range of division plane defects including misplaced, split, and tilted septa (Fig. 7D and E). These defects were not simply due to the increased width of *pak1-as*

cells, as we did not observe similar phenotypes or localization defects for *GFP-mid1-Nter rga4*Δ cells (Fig. 7C-E). We conclude that Pak1 phosphorylates the N-terminus of Mid1 to promote proper cytokinesis.

The cytokinesis proteins Cdc15 and Cyk3, which physically associate with each other (Roberts-Galbraith et al., 2010), were also phosphorylated in a Pak1-dependent manner in cells. Cdc15 is an essential and heavily phosphorylated membrane-binding protein that connects multiple cytokinesis factors including Cyk3 to the CAR (Roberts-Galbraith et al., 2010; Martín-García et al., 2014; Kettenbach et al., 2015; Ren et al., 2015; Willet et al., 2015; Lee et al., 2018). We identified Pak1-dependent phosphorylation of S666 between the F-BAR and SH3 domains of Cdc15 (Fig. 8A). Using purified proteins, we found that Pak1 phosphorylates both Cdc15 and Cyk3 *in vitro* (Fig. 8B and S3D). Cdc15 and Cyk3 localize to cell ends during interphase and to the CAR during cytokinesis. Cyk3 localization was unaffected in *pak1-as* cells (Fig. S3C), but we found that some Cdc15 remained at cell tips during cytokinesis in *pak1-as* but not wild-type cells (Fig. 8C). We used time-lapse microscopy to investigate this phenotype in more detail. In wild-type cells, GFP-Cdc15 was fully recruited away from cell tips and into the CAR at cytokinesis (Fig. 8D). In contrast, most *pak1-as* cells underwent cytokinesis with residual GFP-Cdc15 at the cell tips (Fig. 8D-E). This result suggests that Pak1 alters Cdc15 dynamics to promote its redistribution to the cell middle. Consistent with this notion, we observed stable Cdc15 puncta at the tips of *pak1-as* cells, but not wild-type cells (Fig. 8F-G). Taken together, these results show that Pak1 directly phosphorylates Cdc15 to promote its concentration in the CAR for cytokinesis.

Pak1 phosphorylates RNA-binding protein Sts5 for cell separation

We were intrigued by the identification of Sts5 as a potential Pak1 substrate from our screen. Sts5 forms ribonucleoprotein (RNP) granules in cells through its N-terminal intrinsically disordered region (IDR) and its C-terminal RNA binding domain (Toda et al., 1996; Vaggi et al., 2013; Nuñez et al., 2016). These granules associate with other factors and mature into P-bodies under environmental stresses such as glucose starvation (Nuñez et al., 2016). Sts5 has been functionally linked to septation, and Sts5 granule formation in cells was recently shown to be regulated by the cell polarity kinase Orb6 (Nuñez et al., 2016). Our screen identified two Pak1-dependent phosphorylation sites in residues S261 and S264 of the Sts5 IDR (Fig. 9A). These sites were less phosphorylated in *pak1-as* cells compared to wild-type, and their phosphorylation was further reduced upon addition of 3-Brb-PP1 inhibitor (Fig. 5C). Addition of this inhibitor also induced the cell septation defects of *pak1-as* cells, making Sts5 a candidate substrate for Pak1 function in cell division. Using purified proteins, we found that Pak1 directly phosphorylates Sts5 *in vitro* (Fig. 9B). To determine if phosphorylation of Sts5 by Pak1 alters its propensity to form RNP granules, we used live-cell microscopy of Sts5-mNG in *pak1-as* cells. Consistent with past work (Vaggi et al., 2013; Nuñez et al., 2016), we found that Sts5 localizes diffusively in the cytoplasm of wild-type cells during most of the cell cycle except for mitosis, when it forms granules (Fig. 9C). In *pak1-as* cells, Sts5 localizes to granules throughout the cell cycle (Fig. 9C). Thus, Pak1 phosphorylates Sts5 and regulates its assembly into granules. We considered the possibility that unregulated Sts5 granule assembly might underlie the septation defect in *pak1-as* cells. Consistent with this model, *sts5*Δ largely suppressed the septation defect of *pak1-as* cells (Fig. 9D).

We further tested Pak1 regulation of Sts5 by mutating the S261 and S264 phosphorylation sites to alanine, thereby preventing their phosphorylation by Pak1. The Sts5-S261A, S264A mutant reduced phosphorylation by Pak1 *in vitro* (Fig. 9E), and displayed constitutive granule assembly in cells (Fig. 9F). We conclude that Pak1 phosphorylates the Sts5 IDR to prevent the formation of RNA granules. Defects in this regulation contribute to septation defects in the *pak1-as* mutant, providing an unanticipated mechanism linking Pak1 to cell division.

DISCUSSION

Our study began with a search for cell polarity kinases that function in cytokinesis, and revealed recruitment of Pak1 and its upstream activator Cdc42 to the assembling CAR for cytokinesis. We found new functions for Pak1 in cytokinesis and septation, and used large-scale phosphoproteomics to identify key substrates that are directly phosphorylated by Pak1 *in vitro* and are regulated by Pak1 in cells (Figure 10). Our findings reveal new mechanisms for Pak1 function and raise additional questions. Here, we discuss each class of substrates, along with directions for future work.

Pak1 in cell polarity

From the list of proteins that are phosphorylated in a Pak1-dependent manner in cells, we selected three cell polarity proteins for additional experiments. We note that additional proteins with links to cell polarity were identified in our screen and likely contribute to Pak1-dependent regulation of polarized growth. Both Tea3 and Scd1 were expected substrates of Pak1. Past work has shown that Pak1 phosphorylates Tea3 (Geymonat et al., 2018), and the budding yeast Scd1-related protein Cdc24 is a well-characterized substrate of the PAK Cla4 (Gulli et al., 2000; Wai et al., 2009; Kuo et al., 2014). However, our observation that Pak1 regulates nuclear localization of its substrate Scd1 was unexpected. In budding yeast, regulated release of Cdc24 from the nucleus contributes to polarity establishment (Gulli et al., 2000; Shimada et al., 2000), and our work suggests a parallel mechanism might operate with Scd1 in fission yeast. Phosphorylation by Pak1 could directly regulate nuclear shuttling, or alternatively weaken anchoring of Scd1 at cell tips.

While Pak1 regulates cell tip-localized polarity factors such as Tea3 and Scd1, we also discovered that Pak1 phosphorylates the Cdc42 GAP Rga4, which localizes to the cell middle. This localization pattern has been proposed to prevent Cdc42-directed growth at cell sides, thereby restricting bipolar growth to the cell tips (Das et al., 2007; Tatebe et al., 2008; Kokkoris et al., 2014). We found that reduced Pak1 kinase activity altered Rga4 clustering properties. Several proteins including Rga4 form non-overlapping cortical puncta at the cell middle (Morrell et al., 2004; Wu et al., 2006, Tatebe et al., 2008; Deng et al., 2013). How these structures are excluded from cell tips has been a long-standing question. The cell polarity kinase Pom1 has been identified as one such tip exclusion factor, but Rga4 and other cortical puncta are still excluded from one cell tip in *pom1*Δ mutants (Tatebe et al., 2008; Martin and Berthelot-Grosjean, 2009; Moseley et al., 2009; Deng et al., 2013; Padte et al., 2006). Our finding that Rga4 enriches at cell tips in *pom1-as pak1-as* double mutant cells indicates that these two polarity kinases collaborate as tip exclusion factors. It also demonstrates that cells require active repulsion of Rga4 at cell tips to sustain polarized growth, as Rga4 has an apparent affinity for cell tips in the absence of such kinase-driven repulsion. We note that Pom1, unlike Pak1, has not been shown to phosphorylate Rga4 directly. Therefore, additional work will be needed to determine if the combined effects of Pom1 and Pak1 represent additive phosphorylation of Rga4. The underlying mechanisms, which include altered clustering activity due to Pak1, are likely to be informative for spatial control of Cdc42-directed polarized growth in other cell types.

Novel substrates explain the role of Pak1 in cytokinesis

We found that Pak1 is recruited to the assembling CAR during mitosis, concomitant with the appearance of activated Cdc42 at this site. The colocalization between Pak1 and CAR marker Rlc1 was not complete, suggesting that Pak1 may contribute to the coordination of CAR assembly in time and space, as opposed to representing a structural component of nodes and the CAR. We note that nodes have been shown to exhibit heterogeneity in their components,

meaning that not all nodes contain the exact same set of proteins at any given time (Laporte et al., 2011). The signals that organize distinct cytoskeletal structures during interphase polarized growth might also contribute to robust formation of the CAR from these precursor nodes. The space between nodes as they assemble is likely filled with actin filaments and regulators, and our data suggest that Pak1 localizes in this space and is required for efficient coalescence of nodes into the fully assembled CAR.

Multiple cytokinesis proteins are phosphorylated by Pak1. We confirmed previous reports that Pak1 phosphorylates Rlc1 (Loo and Balasubramanian, 2008), but our phenotypic analysis revealed that other substrates must exist to explain CAR assembly defects in *pak1-as* cells. Thus, we focused on the novel substrates Mid1 and Cdc15, which were identified in our phosphoproteomic screen. Both of these cytokinetic node proteins bind directly to lipids and to other CAR proteins, and physically interact with each other by co-immunoprecipitation and two-hybrid (Lee and Wu, 2012). Mid1 is required for medial position and orientation of nodes and the CAR, and Cdc15 is essential for CAR assembly (Chang et al., 1996; Sohrmann et al., 1996; Paoletti and Chang, 2000; Roberts-Galbraith et al., 2010; Martín-García et al., 2014; Ren et al., 2015; Willet et al., 2019). We found that Pak1 phosphorylates both Mid1 and Cdc15, and these proteins are dysregulated in *pak1-as* cells. Retention of Cdc15 at cell tips in *pak1-as* cells suggests that phosphorylation promotes its dynamic release for redistribution to the cell middle.

We have now shown that Cdc15 and its CAR ligand Cyk3 are phosphorylated by three cell polarity kinases: Pom1, Kin1, and Pak1 (Kettenbach et al., 2015; Lee et al., 2018). Regulation of these CAR proteins by multiple cell polarity kinases indicates a key role for the cell polarity program in the regulation of cell division. Moreover, these three cell polarity kinases phosphorylate largely non-overlapping residues on their shared substrates (Kettenbach et al., 2015; Lee et al., 2018), meaning that they contribute to distinct regulatory steps in this polarity-driven regulation of cell division.

Mid1 is also phosphorylated by multiple protein kinases including Pak1 (Almonacid et al., 2011; Willet et al., 2019). Our work suggests that Pak1 promotes the core function of the Mid1 N-terminus, as this region mis-localizes and becomes non-functional in *pak1-as* cells. These results raise the possibility that PAKs regulate Mid1-related anillin proteins and Cdc15-related F-BAR proteins in other systems (Meitinger et al., 2011; Kim et al., 2017). We also note that additional cytokinesis proteins were identified in our screen for Pak1 substrates, so future work may reveal additional layers for regulation of cytokinesis by Pak1 and its orthologs in other systems.

Septation: RNP aggregation through cell polarity kinases

We discovered that Pak1 phosphorylates Sts5 to inhibit the assembly of RNP granules. Defects in this regulatory step appear to explain the septation defect in *pak1-as* cells treated with inhibitor. Recent work identified a similar role for the NDR/LATS kinase Orb6 (Nuñez et al., 2016). Mutation of the two identified Pak1 phosphorylation sites in the Sts5 IDR led to constitutive granule assembly. This phenotype is consistent with the ability of such domains to mediate assembly of biomolecular condensates akin to liquid-liquid phase separations (Hyman et al., 2014). Phosphorylation is emerging as a common regulatory mechanism to inhibit IDR condensation (Rai et al., 2018), but additional experiments will be required to test this hypothesis for Sts5, Pak1, and Orb6. It is interesting to note that all three of these proteins were identified in the same genetic screen for round and orb-shaped mutants (*pak1* is also called *orb2*; *sts5* is also called *orb4*) (Verde et al., 1995). The exact composition of Sts5 RNP granules is not well defined, but several RNAs with functional connections to septation and polarized growth are misregulated in *sts5*Δ cells (Nuñez et al., 2016). Fission yeast has served as a strong model system for studying cell polarity, and past work has focused heavily on mechanisms connecting to the actin and microtubule cytoskeletons (Chang and Martin, 2009). We propose that future work into the connection between Pak1, Orb6, and Sts5 may reveal

distinct polarity mechanisms, related to RNP granules, that control cell geometry in fission yeast and potentially other systems.

Connecting polarized growth and cell division through signaling proteins

Cell polarity orients cytoskeletal filaments toward spatial landmarks, directing local cell growth (Tojkander et al., 2012; Chiou et al., 2017; Omotade et al., 2017). Protein kinases play key roles in cell polarity by translating spatial signals into regulation of cytoskeletal proteins including actin and myosin. At cell division, the actomyosin machinery dramatically reorganizes into a cytokinetic ring that constricts to separate the dividing cells (Wu et al., 2003; Wu et al., 2006). Our work shows that PAK kinases act beyond polarized growth in multiple steps of cell division including CAR assembly (Fig. 10). Our past work also identified roles for the cell polarity kinases Pom1 and Kin1 in regulating the CAR during constriction (Lee et al., 2018). These combined studies suggest that cell polarity signaling pathways may play critical roles throughout the cytoskeletal rearrangements that occur during cytokinesis and cell division. We have identified the underlying substrates and signaling mechanisms in fission yeast, but these findings and pathways might also operate in a range of eukaryotic cells.

ACKNOWLEDGEMENTS

We thank members of the Moseley laboratory for comments on the manuscript, as well as L. Myers at Dartmouth for help with *in vitro* kinase assays, A. Lavanway for assistance with microscopy, and M. Adamo for help with mass spectrometry data. We thank the Biomolecular Targeting Core (BioMT) (P20-GM113132) and the Imaging Facility at Dartmouth for use of equipment; and J.-Q. Wu, A. Paoletti, J. Gregan for sharing strains.

This work was supported by grants from the American Cancer Society (RSG-15-140-01) and the National Institute of General Medical Sciences (R01GM099774) to J.B.M, and by grants from NIH/NIGMS (R35GM119455, P20GM113132) to A.N.K., and by the NCCC support grant from NIH/NCI (P30CA023108). The Orbitrap Fusion Tribrid mass spectrometer was acquired with support from NIH (S10-OD016212).

The authors declare no competing financial interests.

Author contributions: J.B. Moseley and J.O. Magliozzi conceived of the study; J. Sears and A.N. Kettenbach performed and analyzed mass spectrometry experiments; J.O. Magliozzi, M. Brady, and H.E. Opalko performed all other experiments; all authors analyzed the data; J.B. Moseley and J.O. Magliozzi wrote the manuscript; all authors edited the manuscript.

FIGURE LEGENDS

Figure 1: Cell polarity kinase Pak1 and activated Cdc42 localize to the cell division site
(A) Localization of the indicated protein kinases during distinct stages of cell division. Each strain also expressed Rlc1-mRuby2 and Sad1-mCherry to mark cell division cycle timing. Red box highlights Pak1-mEGFP localization during CAR assembly. **(B)** Colocalization of Pak1-mEGFP and Rlc1-mRuby2 by Airyscan confocal microscopy. Insets are enlarged views of the boxed regions. **(C)** Localization of Pak1 and GTP-Cdc42 at the assembling CAR. Graph shows quantification of CAR localization. All images are maximum intensity projections, Scale bars, 2 µm.

Figure 2: *pak1* mutants have cytokinesis defects
(A) Quantification of CAR formation timing for the indicated strains. Values are mean ± SD. **p <0.01, ***p <0.001 **(B)** Serial-dilution growth assays for each indicated strain. Strains were grown at either 25°C or 37°C for 3-4 days on YE4S plates. **(C)** Representative images of strains grown at 25°C and stained with Blankophor. Red arrows indicate cytokinesis defects in double-mutant backgrounds. Scale bar, 5 µm. **(D)** Percentage of cells that display a division septum at a cell tip. Cells were grown at 25°C overnight and imaged, or switched to 32°C or 37°C for six and three hours before imaging, respectively. n > 30 dividing cells for each strain and condition. **(E)** Quantification of percentage of cells with multiple septa. Cells were imaged at 25°C. Values are the mean ± SD from three biological replicates, (n > 60 cells each).

Figure 3: Inhibition of *pak1-as* leads to cell separation defects
(A) Representative images of *pak1-as* cells treated with 30µM 3-Brb-PP1 or methanol for 60 minutes, and stained with Blankophor. Scale bar, 5 µm. **(B)** Quantification of septation index from three biological replicates from the indicated conditions (n > 150 cells each). ***p <0.001.

Figure 4: Novel *pak1* mutant defects are independent of Rlc1 S35 phosphorylation
(A) *In vitro* kinase assay using full-length Pak1 and Rlc1 purified from bacteria. The indicated proteins were mixed with γ-^{32}P-ATP, separated by SDS-PAGE and visualized by autoradiography. **(B)** Images of indicated strains stained with Blankophor. Scale bar, 5 µm. **(C)** Quantification of CAR formation timing for each indicated strain. Values are mean ± SD. **(D)** Quantification of septation index from three biological replicates, (n > 150 cells each). **(E)** Serial-dilution growth assays. The indicated strains were grown at either 25°C or 37°C for 3-4 days on YE4S plates.

Figure 5: Large-scale phosphoproteomic screen reveals novel Pak1 substrates
(A) Schematic of phosphoproteomic screen. Cell cultures were treated with either 30µM 3-Brb-PP1 or methanol for 15 minutes prior to harvesting and lysis. **(B)** List of putative Pak1 substrates involved in cell polarity and cytokinesis. For each phosphopeptide, the abundance ratio between *pak1-as* and wild-type (both in methanol) was $\log_2$-transformed. **(C)** List of Pak1 substrates involved in septation. Values for "Ratio" were computed as in the previous panel. For each phosphopeptide, "Ratio (+)" is the abundance ratio between *pak1-as* treated with 3-BrB-PP1 versus methanol.

Figure 6: Pak1 phosphorylates proteins involved in polarized growth
(A) *In vitro* kinase assays. The indicated proteins were purified from bacteria, mixed with Pak1 in the presence of γ-^{32}P-ATP, separated by SDS-PAGE and visualized by autoradiography. **(B)** Left: localization of Scd1-mNG in the indicated strains. Images are deconvolved sum projections. Scale bar, 2 µm. Right: quantification of Scd1-mNG nuclear signal. Values are the

mean ± SD from three biological replicates (n > 40 cells each). **p <0.01. **(C)** Localization of Tea3-mEGFP in the indicated strains. Top row images are deconvolved maximum intensity projections; bottom row images are single focal plane DIC. Scale bar, 5 µm. **(D)** Airyscan confocal microscopy images of Rga4-mNG. Images are maximum intensity projections. Scale bar, 2 µm. Fluorescence intensity quantification of Rga4-mNG puncta from sum projections of the top half of cells (n > 250 puncta each). Values are the mean ± SD of background subtracted fluorescence intensity using equal sized ROI, ****p <0.0001. **(E)** Left: Images of Rga4-GFP in the indicated strains treated with 30µM 3-Brb-PP1 for 15 minutes prior to imaging. Images are deconvolved maximum intensity projections. Red arrow indicates cell with Rga4-GFP signal at both cell tips. Scale bar, 2 µm. Right: Quantification of Rga4-GFP signal at both cell tips. Values are the mean ± SD from three biological replicates (n > 50 cells each), *p <0.05, ****p <0.0001.

Figure 7: Pak1 phosphorylates contractile ring protein Mid1 to ensure proper cytokinesis
(A) Schematic of Mid1 domain layout. Red lines indicate Pak1-dependent phosphorylation sites identified in our screen. **(B)** *In vitro* kinase assays. The indicated proteins were expressed and purified from bacteria, mixed with γ-^{32}P-ATP, separated by SDS-PAGE, and visualized by autoradiography. **(C)** Localization of GFP-Mid1Nter. Deconvolved single focal plane images are shown. Insets are enlarged views of boxed region. Scale bar, 3 µm. **(D)** Images of GFP-Mid1Nter cells stained with Blankophor. Scale bar, 5 µm. **(E)** Quantification of aberrant cytokinesis consisting of tilted, split, tip and multiple septa judged from Blankophor stained cells. Values are the mean ± SD from three biological replicates (n ≥ 75 cells each), ****p <0.0001.

Figure 8: Pak1 regulates F-BAR protein Cdc15 localization and dynamics
(A) Schematic of Cdc15 domain layout. Red line indicates Pak1-dependent phosphorylation site identified in our screen. **(B)** *In vitro* kinase assays. The indicated proteins were expressed and purified from bacteria, mixed with γ-^{32}P-ATP, separated by SDS-PAGE, and visualized by autoradiography. **(C)** Images of GFP-Cdc15 Sad1-mEGFP during cytokinesis. Arrows indicate Cdc15 localization at cell tips during cytokinesis in *pak1-as* cells. Images are maximum intensity projections. **(D)** Representative time-lapse montage of GFP-Cdc15 during cytokinesis. Arrow indicates Cdc15 localization at cell tips. Medial focal plane images are shown. **(E)** Quantification of cells with GFP-Cdc15 signal at cell tips during cytokinesis. Values are the mean ± SD from three biological replicates (n > 50 cells each), ***p <0.001. **(F)** Single focal plane images of GFP-Cdc15 from time-lapse microscopy. Whole cell image represents time point zero. Insets are cell tip images over time from the boxed region. Scale bars, 2 µm. **(G)** Quantification of cells with stable GFP-Cdc15 puncta at cell tips. Values are the mean ± SD from three biological replicates (n > 50 cells each), ***p <0.001.

Figure 9: Pak1 phosphorylates RNA-binding protein Sts5 to inhibit granule assembly
(A) Schematic of Sts5 domain layout. Red lines indicate Pak1-dependent phosphorylation sites identified in our screen. **(B)** *In vitro* kinase assays. The indicated proteins were expressed and purified from bacteria, mixed with γ-^{32}P-ATP, separated by SDS-PAGE, and visualized by autoradiography. **(C)** Sts5-mNG localization in the indicated strains. Red arrow indicates Sts5-mNG granules in mitotic wild-type cell. Images are either deconvolved maximum intensity projections of the cell middle or single focal plane DIC. **(D)** Quantification of septation index of indicated strains from three biological replicates, (n > 150 cells each). **p <0.01 ***p <0.001. **(E)** *In vitro* kinase assays performed as in panel B. GST-Sts5 protein loading was assessed using SDS-PAGE followed by silver staining. **(F)** Localization of the indicated Sts5-mNG constructs. Images are deconvolved maximum intensity projections of the cell middle. Scale bars, 2 µm.

Figure 10: Model for Pak1 regulation of three distinct cellular processes

Diagram showing key Pak1 substrates for cell polarity, cytokinesis, and septation. See text for additional discussion.

Supplemental Figure S1: Pak1 oscillations between cell tips
(A) Representative images of Pak1-mNG and CRIB-3xGFP during the cell cycle. Images are deconvolved maximum intensity projections. **(B)** Localization of Pak1-mNG oscillating between growing cell tips. Montage of images acquired every two minutes. * denotes Pak1-mNG signal oscillation. Scale bars, 2 µm.

Supplemental Figure S2: Additional characterization of *pak1* mutant phenotypes
(A) Images of wild-type and *pak1* mutant cells stained with Blankophor. Quantification of cell width in *pak1* mutants. Values are the mean ± SD, **** p <0.0001. **(B)** DIC images of *pak1-as* cells treated overnight at 25°C with either 30µM 3-Brb-PP1 or methanol. **(C)** Time lapse imaging montage of Rlc1-mNG Sad1-mEGFP localization during cytokinesis. SPB splitting represents time zero for monitoring CAR formation. **(D)** Quantification of CAR formation for each indicated strain. For *pak1-as* 3-Brb-PP1, cells were briefly incubated with 30µM 3-Brb-PP1 and then immediately imaged on YE4S agarose pads containing 30µM 3-Brb-PP1. Values are mean ± SD. ***p <0.001, ****p <0.0001. **(E)** Quantification of CAR dynamics in the indicated strains (n ≥ 18 cells each). Values are mean ± SD. **p <0.01, ***p <0.001, ****p <0.0001. **(F)** Top: serial-dilution growth assays for each indicated strain. Strains were grown at either 25°C or 37°C for 3-4 days on YE4S media. Bottom: images of the indicated strains stained with Blankophor. Scale bars, (A-B, F) 5 µm; (C) 2 µm. **(G)** Quantification of septation index of strains from three biological replicates, (n > 150 cells each). ****p <0.0001.

Supplemental Figure S3: Localization of Pak1 cytokinesis targets
(A) Purified proteins used for *in vitro* kinase assays. Proteins were separated by SDS-PAGE followed by coomassie staining. Proteins were loaded at concentrations used for *in vitro* kinase assays, and asterisks denote correct protein band. Middle panel shows separate gel with higher loading volume for GST-Tea3 to confirm band size. **(B)** Localization of Mid1-mNG in the indicated strains. Images are maximum intensity projections acquired by spinning disc confocal microscopy. Scale bars, 5 µm. **(C)** Localization of Cyk3-GFP in the indicated strains. Images are either deconvolved maximum intensity projections or single focal plane DIC. **(D)** *In vitro* kinase assays using indicated proteins all purified from bacteria. Assays were treated with γ-^{32}P-ATP, separated by SDS-PAGE and visualized by autoradiography.

Table S1: List of yeast strains and plasmids used in this study

Table S2: Phosphoproteomic data set

MATERIALS AND METHODS

Strain construction and media

Standard *S. pombe* media and methods were used (Moreno et al., 1991). Strains used in this study are listed in Table S1. PCR-based homologous recombination was performed for chromosomal tagging and deletion (Bahler et al., 1998). The *pak1-as* (M460A) strain was generated and shared by Juro Gregan lab (Cipak et al., 2011). The non-phosphorylatable *rlc1* sequences were generated by site-directed mutagenesis using QuikChange II mutagenesis (Stratagene) according to the manufacturers protocol, and integrated into the *leu1* locus of JM837 (*leu1-32*) using pJK148. Strains with *rlc1* sequences integrated at the *leu1* locus were crossed to an *rlc1*Δ strain to eliminate the copy at the endogenous locus. Wild-type pJK148-*rlc1*+ fully rescued all *rlc1*Δ phenotypes. The *sts5(S261A,S264A)* mutant allele was synthesized as a gBlocks Gene Fragment (Integrated DNA Technologies), and then inserted into the PCR-linearized fragment from pJK148-*Psts5-sts5-mNeonGreen-Tadh1* plasmid by repliQa HiFi Assembly Mix (Quantabio) according to the manufacturer's protocol. The wild-type and non-phosphorylatable *sts5* alleles were integrated into the *leu1* locus of an *sts5*Δ strain. The wild-type pJK148-*sts5-mNeonGreen* integrated in this manner rescued all *sts5*Δ phenotypes. All plasmids were sequenced by Sanger Sequencing for verification. For growth assays, cells were spotted by 10-fold serial dilutions on YE4S plates and were incubated at 25°C or 37°C for 3-4 days before scanning.

Large-Scale Phosphoproteomic Screen

The strains used for phosphoproteomic screen were JM366 (972) and JM4787 (*pak1::ClonNatR pak1-as(M460A)-HphR*). Cells were grown in YE4S at 32°C for at least 8 generations and treated for 15 minutes with 30μM 3-Brb-PP1 (3-[(3-Bromophenyl)methyl]-1-(1,1-dimethylethyl)-1H-pyrazolo[3,4-d]pyrimidin-4-amine (Abcam), while control culture was treated with equal volume of methanol. Each culture volume was 1 liter YE4S. The cultures were then harvested by 10-minute centrifugation at 8,000 g at 4°C, washed once with 200 mL ice-cold 1x PBS, and then centrifuged again. The remaining cell pellet was weighed and resuspended in a 1:1 ratio with ice-cold 1x PBS with a protease inhibitor tablet (Roche Life Sciences) and 1mM PMSF. The cells were then lysed by two minutes of grinding in a prechilled coffee bean grinder; lysis efficiency was ≈ 80% as judged by microscopy.

Yeast powder was resuspecnded in ice-cold lysis buffer ((8 M urea, 25 mM Tris-HCl pH 8.6, 150 mM NaCl, phosphatase inhibitors (2.5 mM beta-glycerophosphate, 1 mM sodium fluoride, 1 mM sodium orthovanadate, 1 mM sodium molybdate) and protease inhibitors (1 mini-Complete EDTA-free tablet per 10 ml lysis buffer; Roche Life Sciences)) and sonicated three times for 15 seconds each with intermittent cooling on ice. Lysates were centrifuged at 15,000 x g for 30 minutes at 4°C. Supernatants were transferred to a new tube and the protein concentration was determined using a BCA assay (Pierce/ThermoFisher Scientific). For reduction, DTT was added to the lysates to a final concentration of 5 mM and incubated for 30 min at 55˚C. Afterwards, lysates were cooled to room temperate and alkylated with 15 mM iodoacetamide at room temperature for 45 min. The alkylation was then quenched by the addition of an additional 5 mM DTT. After 6-fold dilution with 25 mM Tris-HCl pH 8, the samples were digested overnight at 37˚C with 1:100 (w/w) trypsin. The next day, the digest was stopped by the addition of 0.25% TFA (final v/v), centrifuged at 3500 x g for 30 minutes at room temperature to pellet precipitated lipids, and peptides were desalted on a 500 mg (sorbent weight) SPE C18 cartridge (Grace-Davidson). Peptides were lyophilized and stored at -80°C until further use.

Phosphopeptide purification was performed as previously described (Kettenbach and Gerber, 2011). Briefly, peptides were resuspended in 1.5 M lactic acid in 50% ACN ("binding solution"). Titanium dioxide microspheres were added and vortexed by affixing to the top of a vortex mixer on the highest speed setting at room temperature for 1 hour. Afterwards, microspheres were washed twice with binding solution and three times with 50% ACN / 0.1% TFA. Peptides were eluted twice with 50 mM KH_2PO_4 (adjusted to pH 10 with ammonium hydroxide). Peptide elutions were combined, quenched with 50% ACN / 5% formic acid, dried and desalted on a µHLB OASIS C_{18} desalting plate (Waters). Phosphopeptide enrichment was repeated once.

Phosphopeptides were resuspended in 133 mM HEPES (SIGMA) pH 8.5 and 20% acetonitrile (ACN) (Burdick & Jackson). Peptides were transferred to dried, individual TMT reagent (ThermoFisher Scientific), and vortexed to mix reagent and peptides. After 1 hr at room temperature, each reaction was quenched with 3 µl of 500 mM ammonium bicarbonate solution for 10 minutes, mixed, diluted 3-fold with 0.1% TFA in water, and desalted using C_{18} solid phase extraction cartridges (ThermoFisher Scientific). The desalted multiplex was dried by vacuum centrifugation and separated by offline Pentafluorophenyl (PFP)-based reversed phase HPLC fractionation was performed as previously described (Grassetti et al., 2017).

TMT-labeled samples were analyzed on a Orbitrap Fusion (Senko et al., 2013) mass spectrometer (ThermoScientific) equipped with an Easy-nLC 1000 (ThermoScientific). Peptides were resuspended in 8% methanol / 1% formic acid across a column (45 cm length, 100 µm inner diameter, ReproSil, C_{18} AQ 1.8 µm 120 Å pore) pulled in-house across a 2 hrs gradient from 8% acetonitrile/0.0625% formic acid to 37% acetonitrile/0.0625% formic acid. The Orbitrap Fusion was operated in data-dependent, SPS-MS3 quantification mode (Ting et al., 2011, McAlister et al., 2014) wherein an Orbitrap MS1 scan was taken (scan range = 350 – 1500 m/z, R = 120K, AGC target = 2.5e5, max ion injection time = 100ms), followed by ion trap MS2 scans on the most abundant precursors for 4 seconds (max speed mode, quadrupole isolation = 0.6 m/z, AGC target = 4e3, scan rate = rapid, max ion injection time = 60ms, minimum MS1 scan signal = 5e5 normalized units, charge states = 2, 3 and 4 included, CID collision energy = 33%) and Orbitrap MS3 scans for quantification (R = 15K, AGC target = 2e4, max ion injection time = 125ms, HCD collision energy = 48%, scan range = 120 – 140 m/z, synchronous precursors selected = 10). The raw data files were searched using COMET with a static mass of 229.162932 on peptide N-termini and lysines and 57.02146 Da on cysteines, and a variable mass of 15.99491 Da on methionines and 79.96633 Da on serines, threonines and tyrosine against the target-decoy version of the *S. pombe* FASTA database (UniProt; www.uniprot.org) and filtered to a <1% FDR at the peptide level. Quantification of LC-MS/MS spectra was performed using in house developed software. Phosphopeptide intensities were adjusted based on total TMT reporter ion intensity in each channel and $\log_2$ transformed. P-values were calculated using a two tailed Student's t-test assuming unequal variance. The mass spectrometry proteomics data for the experiments performed in this study have been deposited to the ProteomeXchange Consortium, and can be accessed using PDX accession number PXD014463 (http://proteomecentral.proteomexchange.org/cgi/GetDataset?ID=PXD014463).

Protein purification *and in vitro* kinase assays

Full length Wild-Type and catalytically inactive Pak1, Wild-Type and mutant Rlc1, Tea3, Sts5, Sts5 (S261A,S264A) and fragments of Mid1 (aa 300-450), Scd1 (aa 10-872) and Rga4 (aa 389-1150) were cloned into pGEX6P1 (GST tag) vector (GE Healthcare), expressed in BL21 (DE3 or Rosetta) *E. coli* strains, and purified with glutathione-agarose resin (Sigma-Aldrich) as previously described (Kettenbach et al., 2015). Purified proteins were released from resin by overnight incubation with 3C protease at 4°C or by elution with glutathione. Fragments of Cyk3 (aa 81-388) and Cdc15 (aa 358-928) were purified as previously described (Lee et al., 2018).

In vitro kinase assays were performed by incubating purified proteins in kinase assay buffer (20 mM Tris-HCL pH 7.5, 100 mM NaCl, 10 mM $MgCl_2$, 1 mM $MnCl_2$) supplemented with 10 μM ATP and 2 μCi γ-^{32}P-ATP (blu002z250uc, Perkin Elmer) in 15μL reactions. Reactions were incubated at 30°C and stopped after 30 minutes by adding SDS-PAGE sample buffer (65 mM Tris, pH 6.8, 3% SDS, 10% glycerol, 10% 2-mercaptoethanol) and boiling. Gels were dried for one hour and the signal of γ-^{32}P-ATP was detected via a PhosphorImager scanned by Typhoon 8600 Variable Mode Imager (GE Healthcare). In all cases, bands in the figures correspond to the molecular weight where coomassie-stained protein migrates.

Widefield microscopy and analysis

Cells were imaged in either EMM4S or YE4S at either 25°C, 32°C or 37°C using a DeltaVision imaging system (GE/Applied Precision Ltd.) composed of an IX-inverted widefield microscope (Olympus) with a 100x or 60x oil objective, a CoolSnap HQ2 camera (Photometrics), and an Insight solid-state illumination unit (Applied Precision Ltd.). Images shown as Z stacks were acquired and processed by iterative deconvolution using SoftWoRx software (Applied Precision Ltd.). Single channel fluorescence images are shown in inverted look-up table (LUT). For Fig. S2A, cell width was measured by imaging cells with stained Blankophor and drawing a line across the division plane of septating cells. Fig. 7C is displayed as a deconvolved single focal plane to resolve cortical nodes. All other single focal plane images are non-deconvolved. 30μM 3-Brb-PP1 or an equal volume of methanol was added to cells growing in YE4S media at 32°C for each septation index. For Figs. 3B and 9D, cells were treated with either 3-Brb-PP1 or methanol and fixed in 70% cold ethanol and put in 4°C until imaged with Blankophor stain to assess septation index. The criteria for aberrant cytokinesis analysis in Fig. 7E were tilted septa, multiple septa, tip septa and split septa. For Fig. 8E, we counted cells with detectable GFP-Cdc15 signal at cell tips upon CAR constriction. For Fig. 8G, cells with GFP-Cdc15 puncta that persisted for at least twelve minutes were marked as cells with stable GFP-Cdc15 puncta. For time-lapse imaging, cells were placed onto agarose pads containing the same growth medium and 2% agarose. All image analysis was performed on ImageJ (National Institutes of Health). Statistical differences were assessed by either One-Way ANOVA or Welch's t test using GraphPad.

Spinning disc microscopy and analysis

Images for Figs. 1C, 4C, 8C and S3C were taken with a commercially available spinning-disc confocal system (Micro Video Instruments, Avon, MA) featuring a Nikon Eclipse Ti base equipped with an Andor CSU-W1 two-camera spinning disc module, dual Zyla sCMOS cameras (Andor, South Windsor, CT) an Andor ILE laser module, and a Nikon 100X Plan Apo λ 1.45 oil immerision objective. Statistical differences were assessed by One-Way ANOVA using GraphPad.

Airyscan super resolution microscopy and analysis

Cells were imaged using a Zeiss Airyscan microscope (Figs. 1B and 6D), composed of a Zeiss LSM-880 laser scanning confocal microscope (Zeiss, Oberkochen, Germany) equipped with 100X alpha Plan-Apochromat/NA 1.46 Oil DIC M27 Elyra objective, Airyscan super-resolution module and GaAsp Detectors, and Zen Blue acquisition software using the Super-resolution mode. Z-volumes of 32 slices with 0.17μm spacing through the cell. Airyscan images were processed in Zeiss Zen Blue software, and quantification was performed on sum projections of the top half of cells with Airyscan reconstructed stacks. Rga4-mNG puncta intensity was measured for 8-10 cells with a circular ROI and background subtracted with an identical ROI area. Images in Fig. 1B are Airyscan reconstructed maximum intensity projection Z-stacks of 34 sections with 0.17 μm spacing. Statistical differences were assessed by Welch's t test using GraphPad.

REFERENCES

Almonacid, M., Celton-Morizur, S., Jakubowski, J.L., Dingli, F., Loew, D., Mayeux, A., Chen, J.-S., Gould, K.L., Clifford, D.M., and Paoletti, A. (2011). Temporal control of contractile ring assembly by Plo1 regulation of myosin II recruitment by Mid1/anillin. Curr. Biol. *21*, 473–479.

Almonacid, M., Moseley, J.B., Janvore, J., Mayeux, A., Fraisier, V., Nurse, P., and Paoletti, A. (2009). Spatial control of cytokinesis by Cdr2 kinase and Mid1/anillin nuclear export. Curr. Biol. *19*, 961–966.

Arellano, M., Niccoli, T., and Nurse, P. (2002). Tea3p is a cell end marker activating polarized growth in Schizosaccharomyces pombe. Curr. Biol. *12*, 751–756.

Atkins, B.D., Yoshida, S., Saito, K., Wu, C.-F., Lew, D.J., and Pellman, D. (2013). Inhibition of Cdc42 during mitotic exit is required for cytokinesis. J. Cell Biol. *202*, 231–240.

Bähler, J., and Pringle, J.R. (1998). Pom1p, a fission yeast protein kinase that provides positional information for both polarized growth and cytokinesis. Genes Dev. *12*, 1356–1370.

Bhatia, P., Hachet, O., Hersch, M., Rincon, S.A., Berthelot-Grosjean, M., Dalessi, S., Basterra, L., Bergmann, S., Paoletti, A., and Martin, S.G. (2014). Distinct levels in Pom1 gradients limit Cdr2 activity and localization to time and position division. Cell Cycle *13*, 538–552.

Bokoch, G.M. (2003). Biology of the p21-activated kinases. Annu. Rev. Biochem. *72*, 743–781.

Bringmann, H., and Hyman, A.A. (2005). A cytokinesis furrow is positioned by two consecutive signals. Nature *436*, 731–734.

Cabernard, C., Prehoda, K.E., and Doe, C.Q. (2010). A spindle-independent cleavage furrow positioning pathway. Nature *467*, 91–94.

Celton-Morizur, S., Bordes, N., Fraisier, V., Tran, P.T., and Paoletti, A. (2004). C-terminal anchoring of mid1p to membranes stabilizes cytokinetic ring position in early mitosis in fission yeast. Mol. Cell. Biol. *24*, 10621–10635.

Celton-Morizur, S., Racine, V., Sibarita, J.-B., and Paoletti, A. (2006). Pom1 kinase links division plane position to cell polarity by regulating Mid1p cortical distribution. J. Cell. Sci. *119*, 4710–4718.

Chang, E.C., Barr, M., Wang, Y., Jung, V., Xu, H.P., and Wigler, M.H. (1994). Cooperative interaction of S. pombe proteins required for mating and morphogenesis. Cell *79*, 131–141.

Chang, F., and Martin, S.G. (2009). Shaping fission yeast with microtubules. Cold Spring Harb Perspect Biol *1*, a001347.

Chang, F., Woollard, A., and Nurse, P. (1996). Isolation and characterization of fission yeast mutants defective in the assembly and placement of the contractile actin ring. J. Cell. Sci. *109 (Pt 1)*, 131–142.

Chiou, J.-G., Balasubramanian, M.K., and Lew, D.J. (2017). Cell Polarity in Yeast. Annu. Rev. Cell Dev. Biol. *33*, 77–101.

Coll, P.M., Trillo, Y., Ametzazurra, A., and Perez, P. (2003). Gef1p, a new guanine nucleotide exchange factor for Cdc42p, regulates polarity in Schizosaccharomyces pombe. Mol. Biol. Cell *14*, 313–323.

Das, M., Drake, T., Wiley, D.J., Buchwald, P., Vavylonis, D., and Verde, F. (2012). Oscillatory dynamics of Cdc42 GTPase in the control of polarized growth. Science *337*, 239–243.

Das, M., Wiley, D.J., Medina, S., Vincent, H.A., Larrea, M., Oriolo, A., and Verde, F. (2007). Regulation of cell diameter, For3p localization, and cell symmetry by fission yeast Rho-GAP Rga4p. Mol. Biol. Cell *18*, 2090–2101.

Davies, T., Jordan, S.N., and Canman, J.C. (2016). Cell polarity is on PAR with cytokinesis. Cell Cycle *15*, 1307–1308.

Deng, L., and Moseley, J.B. (2013). Compartmentalized nodes control mitotic entry signaling in fission yeast. Mol. Biol. Cell *24*, 1872–1881.

Drewes, G., and Nurse, P. (2003). The protein kinase kin1, the fission yeast orthologue of mammalian MARK/PAR-1, localises to new cell ends after mitosis and is important for bipolar growth. FEBS Lett. *554*, 45–49.

Endo, M., Shirouzu, M., and Yokoyama, S. (2003). The Cdc42 binding and scaffolding activities of the fission yeast adaptor protein Scd2. J. Biol. Chem. *278*, 843–852.

Eng, K., Naqvi, N.I., Wong, K.C., and Balasubramanian, M.K. (1998). Rng2p, a protein required for cytokinesis in fission yeast, is a component of the actomyosin ring and the spindle pole body. Curr. Biol. *8*, 611–621.

Fantes, P., and Nurse, P. (1977). Control of cell size at division in fission yeast by a growth-modulated size control over nuclear division. Exp. Cell Res. *107*, 377–386.

Geymonat, M., Chessel, A., Dodgson, J., Punter, H., Horns, F., Csikász-Nagy, A., and Salas, R.E. Activation of polarized cell growth by inhibition of cell polarity. bioRxiv *402990*.

Grassetti, A.V., Hards, R., and Gerber, S.A. (2017). Offline pentafluorophenyl (PFP)-RP prefractionation as an alternative to high-pH RP for comprehensive LC-MS/MS proteomics and phosphoproteomics. Anal Bioanal Chem *409*, 4615–4625.

Gulli, M.P., Jaquenoud, M., Shimada, Y., Niederhäuser, G., Wiget, P., and Peter, M. (2000). Phosphorylation of the Cdc42 exchange factor Cdc24 by the PAK-like kinase Cla4 may regulate polarized growth in yeast. Mol. Cell *6*, 1155–1167.

Guzman-Vendrell, M., Baldissard, S., Almonacid, M., Mayeux, A., Paoletti, A., and Moseley, J.B. (2013). Blt1 and Mid1 provide overlapping membrane anchors to position the division plane in fission yeast. Mol. Cell. Biol. *33*, 418–428.

Hayles, J., and Nurse, P. (2001). A journey into space. Nat. Rev. Mol. Cell Biol. *2*, 647–656.

Hirota, K., Tanaka, K., Ohta, K., and Yamamoto, M. (2003). Gef1p and Scd1p, the Two GDP-GTP exchange factors for Cdc42p, form a ring structure that shrinks during cytokinesis in Schizosaccharomyces pombe. Mol. Biol. Cell *14*, 3617–3627.

Hyman, A.A., Weber, C.A., and Jülicher, F. (2014). Liquid-liquid phase separation in biology. Annu. Rev. Cell Dev. Biol. *30*, 39–58.

Jochová, J., Rupes, I., and Streiblová, E. (1991). F-actin contractile rings in protoplasts of the yeast Schizosaccharomyces. Cell Biol. Int. Rep. *15*, 607–610.

Jordan, S.N., Davies, T., Zhuravlev, Y., Dumont, J., Shirasu-Hiza, M., and Canman, J.C. (2016). Cortical PAR polarity proteins promote robust cytokinesis during asymmetric cell division. J. Cell Biol. *212*, 39–49.

Kotak, S., and Gönczy, P. (2013). Mechanisms of spindle positioning: cortical force generators in the limelight. Curr. Opin. Cell Biol. *25*, 741–748.

Kim, H., Johnson, J.M., Lera, R.F., Brahma, S., and Burkard, M.E. (2017). Anillin Phosphorylation Controls Timely Membrane Association and Successful Cytokinesis. PLoS Genet. *13*, e1006511.

Kim, H., Yang, P., Catanuto, P., Verde, F., Lai, H., Du, H., Chang, F., and Marcus, S. (2003). The kelch repeat protein, Tea1, is a potential substrate target of the p21-activated kinase, Shk1, in the fission yeast, Schizosaccharomyces pombe. J. Biol. Chem. *278*, 30074–30082.

Kettenbach, A.N., Deng, L., Wu, Y., Baldissard, S., Adamo, M.E., Gerber, S.A., and Moseley, J.B. (2015). Quantitative phosphoproteomics reveals pathways for coordination of cell growth and division by the conserved fission yeast kinase pom1. Mol. Cell Proteomics *14*, 1275–1287.

Kettenbach, A.N., and Gerber, S.A. (2011). Rapid and reproducible single-stage phosphopeptide enrichment of complex peptide mixtures: application to general and phosphotyrosine-specific phosphoproteomics experiments. Anal. Chem. *83*, 7635–7644.

Kokkoris, K., Gallo Castro, D., and Martin, S.G. (2014). The Tea4-PP1 landmark promotes local growth by dual Cdc42 GEF recruitment and GAP exclusion. J. Cell. Sci. *127*, 2005–2016.

Kuo, C.-C., Savage, N.S., Chen, H., Wu, C.-F., Zyla, T.R., and Lew, D.J. (2014). Inhibitory GEF phosphorylation provides negative feedback in the yeast polarity circuit. Curr. Biol. *24*, 753–759.

La Carbona, S., Allix, C., Philippe, M., and Le Goff, X. (2004). The protein kinase kin1 is required for cellular symmetry in fission yeast. Biol. Cell *96*, 169–179.

Laporte, D., Coffman, V.C., Lee, I.-J., and Wu, J.-Q. (2011). Assembly and architecture of precursor nodes during fission yeast cytokinesis. J. Cell Biol. *192*, 1005–1021.

Lee, I.-J., and Wu, J.-Q. (2012). Characterization of Mid1 domains for targeting and scaffolding in fission yeast cytokinesis. J. Cell. Sci. *125*, 2973–2985.

Lee, M.E., Rusin, S.F., Jenkins, N., Kettenbach, A.N., and Moseley, J.B. (2018). Mechanisms Connecting the Conserved Protein Kinases Ssp1, Kin1, and Pom1 in Fission Yeast Cell Polarity and Division. Curr. Biol. *28*, 84–92.e4.

Levin, D.E., and Bishop, J.M. (1990). A putative protein kinase gene (kin1+) is important for growth polarity in Schizosaccharomyces pombe. Proc. Natl. Acad. Sci. U.S.A. *87*, 8272–8276.

Liu, J., Tang, X., Wang, H., Oliferenko, S., and Balasubramanian, M.K. (2002). The localization of the integral membrane protein Cps1p to the cell division site is dependent on the actomyosin ring and the septation-inducing network in Schizosaccharomyces pombe. Mol. Biol. Cell *13*, 989–1000.

Liu, J., Wang, H., McCollum, D., and Balasubramanian, M.K. (1999). Drc1p/Cps1p, a 1,3-beta-glucan synthase subunit, is essential for division septum assembly in Schizosaccharomyces pombe. Genetics *153*, 1193–1203.

Loo, T.-H., and Balasubramanian, M. (2008). Schizosaccharomyces pombe Pak-related protein, Pak1p/Orb2p, phosphorylates myosin regulatory light chain to inhibit cytokinesis. J. Cell Biol. *183*, 785–793.

Marcus, S., Polverino, A., Chang, E., Robbins, D., Cobb, M.H., and Wigler, M.H. (1995). Shk1, a homolog of the Saccharomyces cerevisiae Ste20 and mammalian p65PAK protein kinases, is a component of a Ras/Cdc42 signaling module in the fission yeast Schizosaccharomyces pombe. Proc. Natl. Acad. Sci. U.S.A. *92*, 6180–6184.

Martín-García, R., Coll, P.M., and Pérez, P. (2014). F-BAR domain protein Rga7 collaborates with Cdc15 and Imp2 to ensure proper cytokinesis in fission yeast. J. Cell. Sci. *127*, 4146–4158.

Martin, S.G., and Berthelot-Grosjean, M. (2009). Polar gradients of the DYRK-family kinase Pom1 couple cell length with the cell cycle. Nature *459*, 852–856.

McAlister, G.C., Nusinow, D.P., Jedrychowski, M.P., Wühr, M., Huttlin, E.L., Erickson, B.K., Rad, R., Haas, W., and Gygi, S.P. (2014). MultiNotch MS3 enables accurate, sensitive, and multiplexed detection of differential expression across cancer cell line proteomes. Anal. Chem. *86*, 7150–7158.

McDonald, N.A., Lind, A.L., Smith, S.E., Li, R., and Gould, K.L. (2017). Nanoscale architecture of the Schizosaccharomyces pombe contractile ring. Elife *6*.

Meitinger, F., Boehm, M.E., Hofmann, A., Hub, B., Zentgraf, H., Lehmann, W.D., and Pereira, G. (2011). Phosphorylation-dependent regulation of the F-BAR protein Hof1 during cytokinesis. Genes Dev. *25*, 875–888.

Morrell, J.L., Nichols, C.B., and Gould, K.L. (2004). The GIN4 family kinase, Cdr2p, acts independently of septins in fission yeast. J. Cell. Sci. *117*, 5293–5302.

Moseley, J.B., Mayeux, A., Paoletti, A., and Nurse, P. (2009). A spatial gradient coordinates cell size and mitotic entry in fission yeast. Nature *459*, 857–860.

Nuñez, I., Rodriguez Pino, M., Wiley, D.J., Das, M.E., Chen, C., Goshima, T., Kume, K., Hirata, D., Toda, T., and Verde, F. (2016). Spatial control of translation repression and polarized growth by conserved NDR kinase Orb6 and RNA-binding protein Sts5. Elife *5*.

Omotade, O.F., Pollitt, S.L., and Zheng, J.Q. (2017). Actin-based growth cone motility and guidance. Mol. Cell. Neurosci. *84*, 4–10.

Padte, N.N., Martin, S.G., Howard, M., and Chang, F. (2006). The cell-end factor pom1p inhibits mid1p in specification of the cell division plane in fission yeast. Curr. Biol. *16*, 2480–2487.

Padmanabhan, A., Bakka, K., Sevugan, M., Naqvi, N.I., D'souza, V., Tang, X., Mishra, M., and Balasubramanian, M.K. (2011). IQGAP-related Rng2p organizes cortical nodes and ensures position of cell division in fission yeast. Curr. Biol. *21*, 467–472.

Paoletti, A., and Chang, F. (2000). Analysis of mid1p, a protein required for placement of the cell division site, reveals a link between the nucleus and the cell surface in fission yeast. Mol. Biol. Cell *11*, 2757–2773.

Pollard, T.D., and Wu, J.-Q. (2010). Understanding cytokinesis: lessons from fission yeast. Nat. Rev. Mol. Cell Biol. *11*, 149–155.

Proctor, S.A., Minc, N., Boudaoud, A., and Chang, F. (2012). Contributions of turgor pressure, the contractile ring, and septum assembly to forces in cytokinesis in fission yeast. Curr. Biol. *22*, 1601–1608.

Rai, A.K., Chen, J.-X., Selbach, M., and Pelkmans, L. (2018). Kinase-controlled phase transition of membraneless organelles in mitosis. Nature *559*, 211–216.

Rappaport, R., Bard, J.B.L., Barlow, P.W., and Kirk, D.L. (2009). Developmental and Cell Biology, 32. (Cambridge, GBR: Cambridge University Press) Available at: http://public.eblib.com/choice/publicfullrecord.aspx?p=4638249 [Accessed September 12, 2018].

Ren, L., Willet, A.H., Roberts-Galbraith, R.H., McDonald, N.A., Feoktistova, A., Chen, J.-S., Huang, H., Guillen, R., Boone, C., Sidhu, S.S., et al. (2015). The Cdc15 and Imp2 SH3 domains cooperatively scaffold a network of proteins that redundantly ensure efficient cell division in fission yeast. Mol. Biol. Cell *26*, 256–269.

Rincon, S.A., Bhatia, P., Bicho, C., Guzman-Vendrell, M., Fraisier, V., Borek, W.E., Alves, F. de L., Dingli, F., Loew, D., Rappsilber, J., et al. (2014). Pom1 regulates the assembly of Cdr2-Mid1 cortical nodes for robust spatial control of cytokinesis. J. Cell Biol. *206*, 61–77.

Roberts-Galbraith, R.H., Ohi, M.D., Ballif, B.A., Chen, J.-S., McLeod, I., McDonald, W.H., Gygi, S.P., Yates, J.R., and Gould, K.L. (2010). Dephosphorylation of F-BAR protein Cdc15 modulates its conformation and stimulates its scaffolding activity at the cell division site. Mol. Cell *39*, 86–99.

Sawin, K.E., Hajibagheri, M.A., and Nurse, P. (1999). Mis-specification of cortical identity in a fission yeast PAK mutant. Curr. Biol. *9*, 1335–1338.

Senko, M.W., Remes, P.M., Canterbury, J.D., Mathur, R., Song, Q., Eliuk, S.M., Mullen, C., Earley, L., Hardman, M., Blethrow, J.D., et al. (2013). Novel parallelized quadrupole/linear ion trap/Orbitrap tribrid mass spectrometer improving proteome coverage and peptide identification rates. Anal. Chem. *85*, 11710–11714.

Shimada, Y., Gulli, M.P., and Peter, M. (2000). Nuclear sequestration of the exchange factor Cdc24 by Far1 regulates cell polarity during yeast mating. Nat. Cell Biol. *2*, 117–124.

Siller, K.H., and Doe, C.Q. (2009). Spindle orientation during asymmetric cell division. Nat. Cell Biol. *11*, 365–374.

Sipiczki, M., and Bozsik, A. (2000). The use of morphomutants to investigate septum formation and cell separation in Schizosaccharomyces pombe. Arch. Microbiol. *174*, 386–392.

Snell, V., and Nurse, P. (1994). Genetic analysis of cell morphogenesis in fission yeast--a role for casein kinase II in the establishment of polarized growth. EMBO J. *13*, 2066–2074.

Sohrmann, M., Fankhauser, C., Brodbeck, C., and Simanis, V. (1996). The dmf1/mid1 gene is essential for correct positioning of the division septum in fission yeast. Genes Dev. *10*, 2707–2719.

Tatebe, H., Nakano, K., Maximo, R., and Shiozaki, K. (2008). Pom1 DYRK regulates localization of the Rga4 GAP to ensure bipolar activation of Cdc42 in fission yeast. Curr. Biol. *18*, 322–330.

Ting, L., Rad, R., Gygi, S.P., and Haas, W. (2011). MS3 eliminates ratio distortion in isobaric multiplexed quantitative proteomics. Nat. Methods *8*, 937–940.

Toda, T., Niwa, H., Nemoto, T., Dhut, S., Eddison, M., Matsusaka, T., Yanagida, M., and Hirata, D. (1996). The fission yeast sts5+ gene is required for maintenance of growth polarity and functionally interacts with protein kinase C and an osmosensing MAP-kinase pathway. J. Cell. Sci. *109 (Pt 9)*, 2331–2342.

Tojkander, S., Gateva, G., and Lappalainen, P. (2012). Actin stress fibers--assembly, dynamics and biological roles. J. Cell. Sci. *125*, 1855–1864.

Vaggi, F., Dodgson, J., Bajpai, A., Chessel, A., Jordán, F., Sato, M., Carazo-Salas, R.E., and Csikász-Nagy, A. (2012). Linkers of cell polarity and cell cycle regulation in the fission yeast protein interaction network. PLoS Comput. Biol. *8*, e1002732.

Vavylonis, D., Wu, J.-Q., Hao, S., O'Shaughnessy, B., and Pollard, T.D. (2008). Assembly mechanism of the contractile ring for cytokinesis by fission yeast. Science *319*, 97–100.

Verde, F., Mata, J., and Nurse, P. (1995). Fission yeast cell morphogenesis: identification of new genes and analysis of their role during the cell cycle. J. Cell Biol. *131*, 1529–1538.

Wai, S.C., Gerber, S.A., and Li, R. (2009). Multisite phosphorylation of the guanine nucleotide exchange factor Cdc24 during yeast cell polarization. PLoS ONE *4*, e6563.

Willet, A.H., DeWitt, A.K., Beckley, J.R., Clifford, D.M., and Gould, K.L. (2019). NDR Kinase Sid2 Drives Anillin-like Mid1 from the Membrane to Promote Cytokinesis and Medial Division Site Placement. Curr. Biol. *29*, 1055–1063.e2.

Willet, A.H., McDonald, N.A., Bohnert, K.A., Baird, M.A., Allen, J.R., Davidson, M.W., and Gould, K.L. (2015). The F-BAR Cdc15 promotes contractile ring formation through the direct recruitment of the formin Cdc12. J. Cell Biol. *208*, 391–399.

Wu, J.-Q., Kuhn, J.R., Kovar, D.R., and Pollard, T.D. (2003). Spatial and temporal pathway for assembly and constriction of the contractile ring in fission yeast cytokinesis. Dev. Cell *5*, 723–734

Wu, J.-Q., Sirotkin, V., Kovar, D.R., Lord, M., Beltzner, C.C., Kuhn, J.R., and Pollard, T.D. (2006). Assembly of the cytokinetic contractile ring from a broad band of nodes in fission yeast. J. Cell Biol. *174*, 391–402.

Yang, P., Pimental, R., Lai, H., and Marcus, S. (1999). Direct activation of the fission yeast PAK Shk1 by the novel SH3 domain protein, Skb5. J. Biol. Chem. *274*, 36052–36057.

Yang, P., Qyang, Y., Bartholomeusz, G., Zhou, X., and Marcus, S. (2003). The novel Rho GTPase-activating protein family protein, Rga8, provides a potential link between Cdc42/p21-activated kinase and Rho signaling pathways in the fission yeast, Schizosaccharomyces pombe. J. Biol. Chem. *278*, 48821–48830.

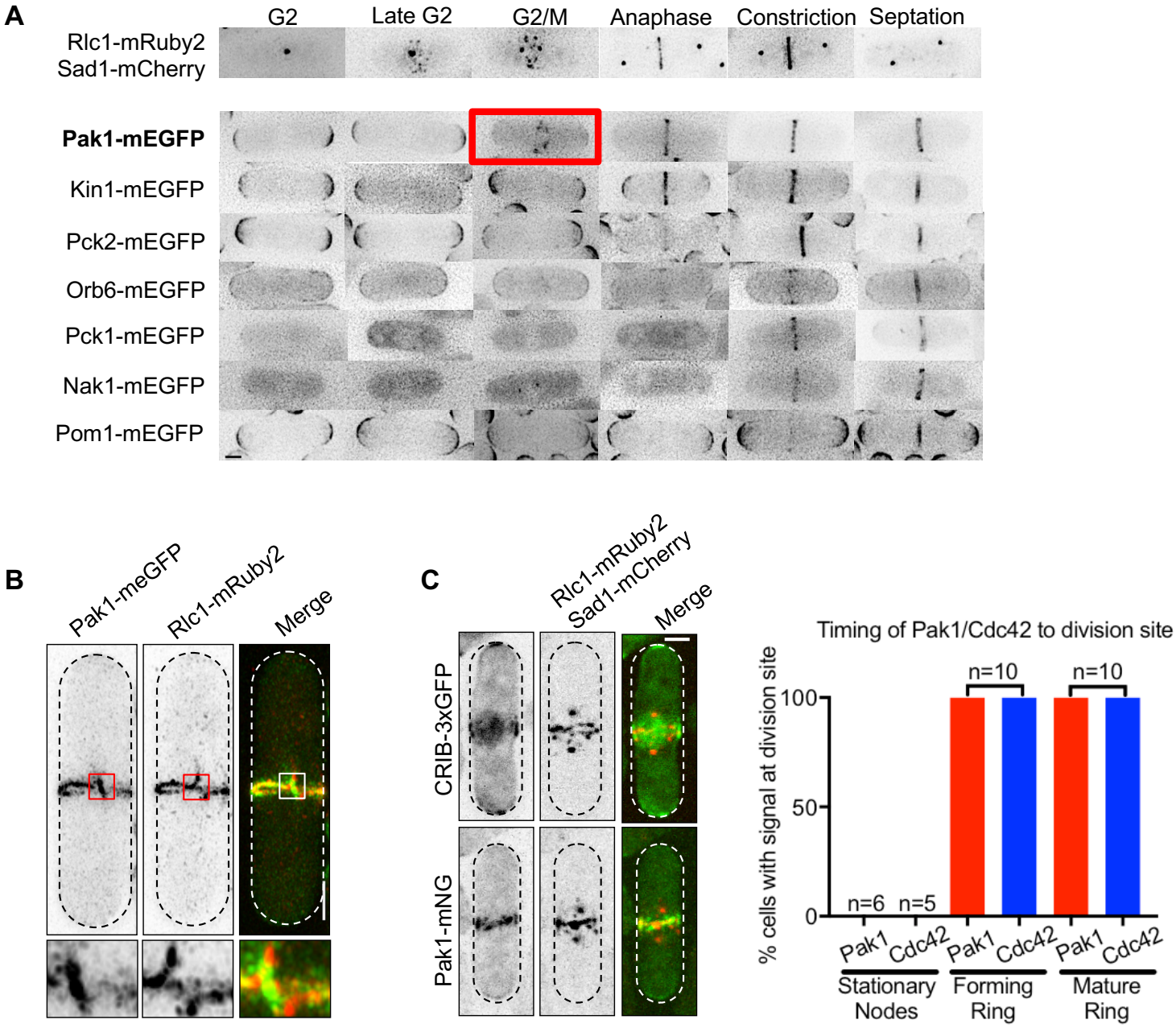
A
G2
Late G2
G2/M
Anaphase
Constriction
Septation
Rlc1-mRuby2
Sad1-mCherry
Pak1-mEGFP
Kin1-mEGFP
Pck2-mEGFP
Orb6-mEGFP
Pck1-mEGFP
Nak1-mEGFP
Pom1-mEGFP
B
Pak1-meGFP
Rlc1-mRuby2
Merge
C
Rlc1-mRuby2
Sad1-mCherry
Merge
CRIB-3xGFP
Pak1-mNG
Timing of Pak1/Cdc42 to division site
% cells with signal at division site
100
50
0
n=6
n=5
n=10
n=10
Pak1
Cdc42
Pak1
Cdc42
Pak1
Cdc42
Stationary Nodes
Forming Ring
Mature Ring

Figure 1

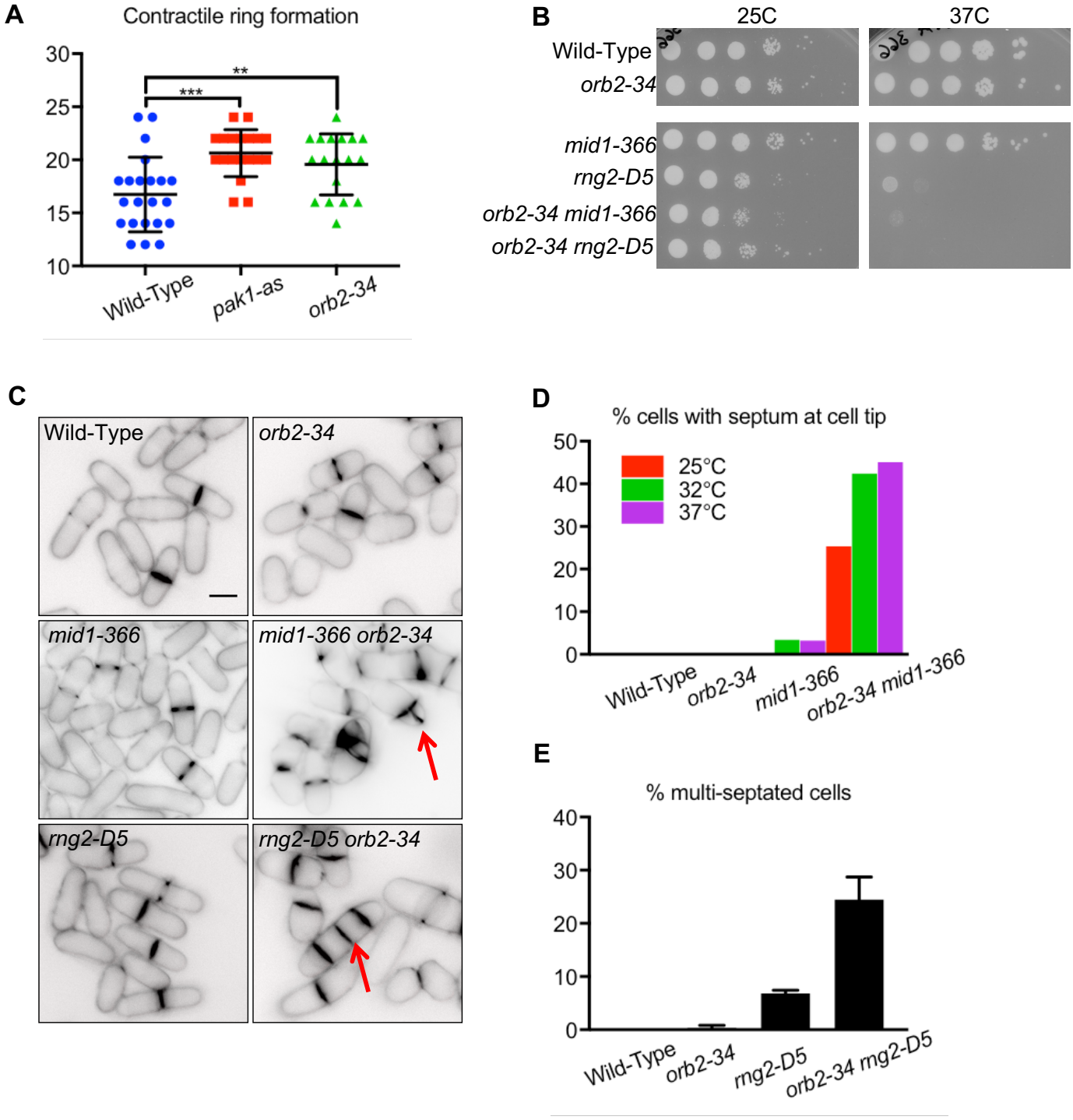
A
Contractile ring formation
30
25
20
15
10
**
***
Wild-Type
pak1-as
orb2-34
B
25C
37C
Wild-Type
orb2-34
mid1-366
rng2-D5
orb2-34 mid1-366
orb2-34 rng2-D5
C
Wild-Type
orb2-34
mid1-366
mid1-366 orb2-34
rng2-D5
rng2-D5 orb2-34
D
% cells with septum at cell tip
50
40
30
20
10
0
25°C
32°C
37°C
Wild-Type
orb2-34
mid1-366
orb2-34 mid1-366
E
% multi-septated cells
40
30
20
10
0
Wild-Type
orb2-34
rng2-D5
orb2-34 rng2-D5

Figure 2

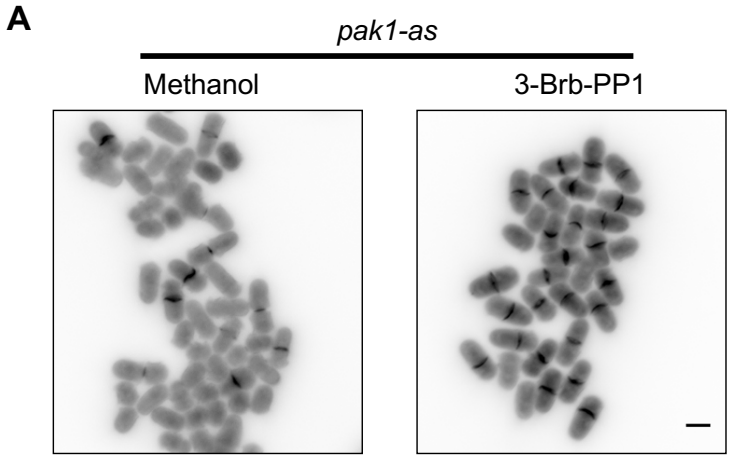
A
pak1-as
Methanol
3-Brb-PP1

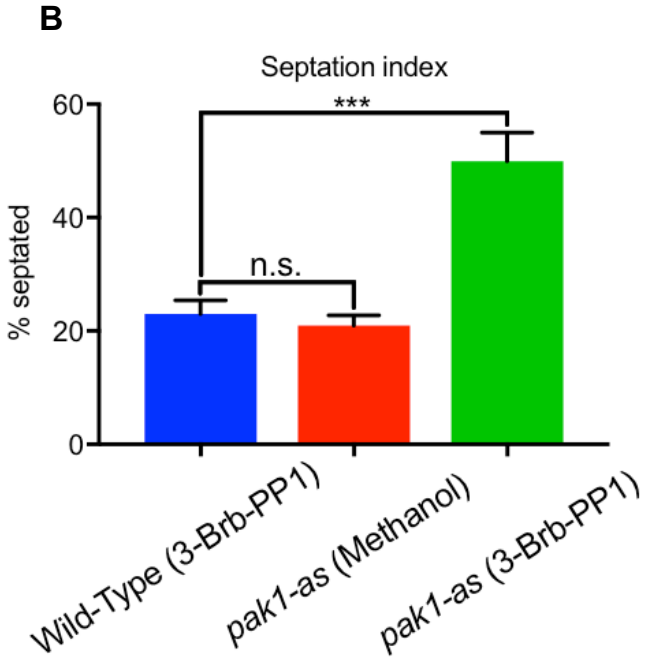
B
Septation index
***
n.s.
% septated
60
40
20
0
Wild-Type (3-Brb-PP1)
pak1-as (Methanol)
pak1-as (3-Brb-PP1)

Figure 3

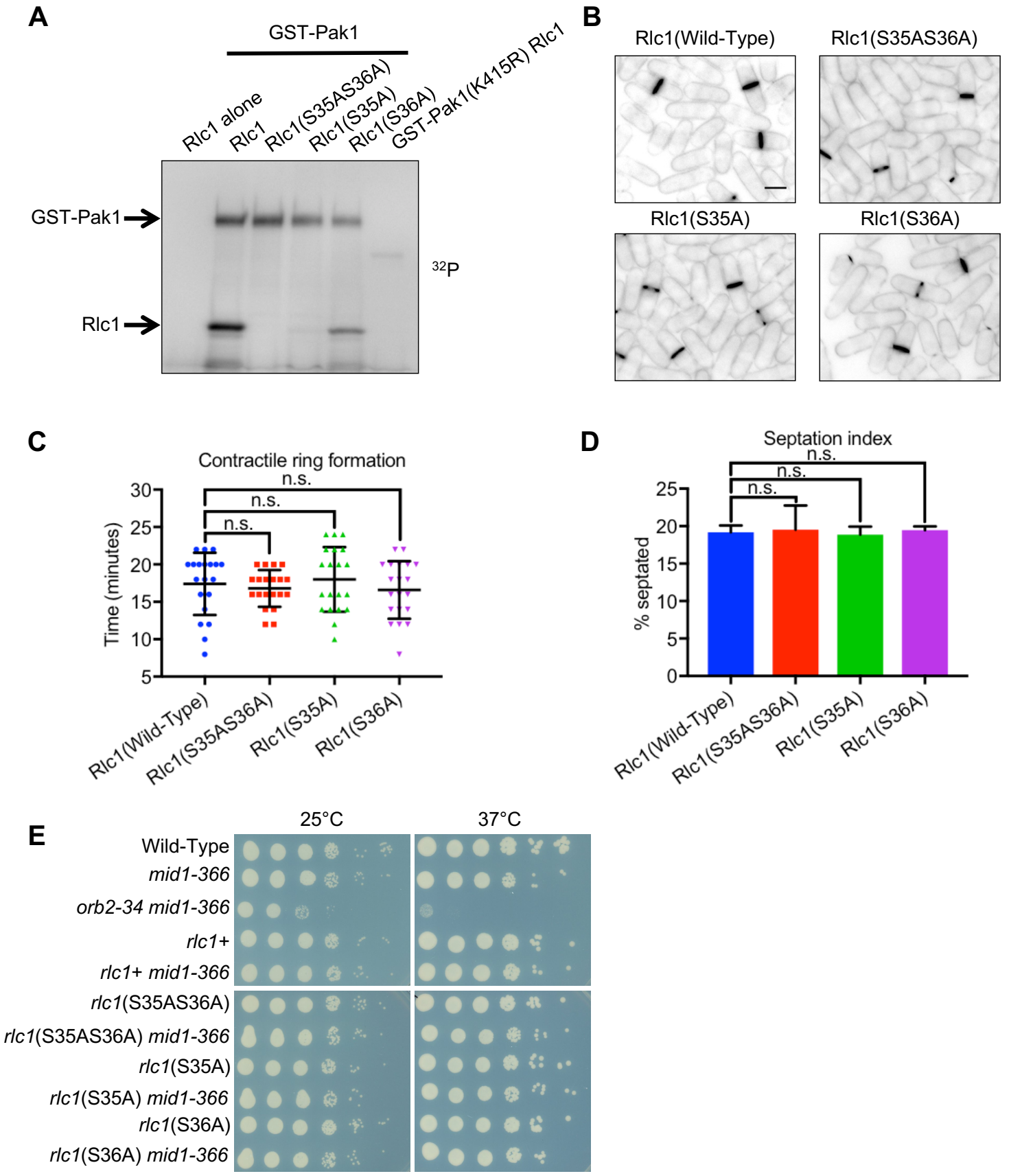
A
GST-Pak1
Rlc1 alone
Rlc1
Rlc1(S35AS36A)
Rlc1(S35A)
Rlc1(S36A)
GST-Pak1(K415R) Rlc1
GST-Pak1
Rlc1
32P
B
Rlc1(Wild-Type)
Rlc1(S35AS36A)
Rlc1(S35A)
Rlc1(S36A)
C
Contractile ring formation
n.s.
n.s.
n.s.
Time (minutes)
30
25
20
15
10
5
Rlc1(Wild-Type)
Rlc1(S35AS36A)
Rlc1(S35A)
Rlc1(S36A)
D
Septation index
n.s.
n.s.
n.s.
% septated
25
20
15
10
5
0
Rlc1(Wild-Type)
Rlc1(S35AS36A)
Rlc1(S35A)
Rlc1(S36A)
E
25°C
37°C
Wild-Type
mid1-366
orb2-34 mid1-366
rlc1+
rlc1+ mid1-366
rlc1(S35AS36A)
rlc1(S35AS36A) mid1-366
rlc1(S35A)
rlc1(S35A) mid1-366
rlc1(S36A)
rlc1(S36A) mid1-366

Figure 4

A

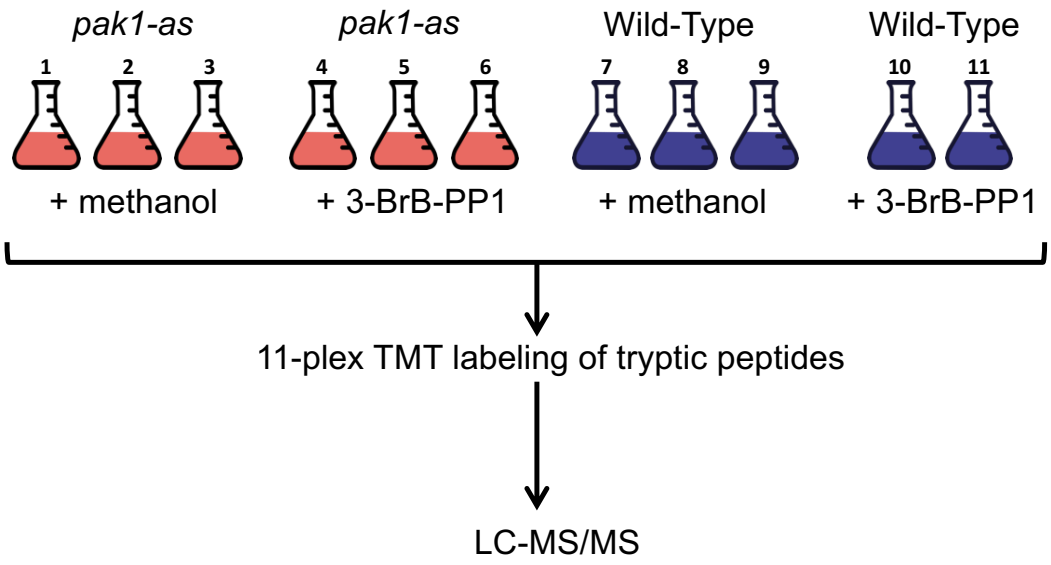

B

	Substrate	Site(s)	Ratio	p-value	Function
Cell Polarity	Pak1	S144	-2.45	0.01	Serine/Threonine Kinase
	Scd1	S573	-2.63	0.001	Cdc42 GEF
	Scd2	S94, S97	-2.20	0.01	Cdc42 scaffold protein
	Tea3	S1045	-2.53	0.003	Cell end maker
	Rga4	S605, S606	-2.00	0.01	RhoGAP, GTPase activating protein
Cytokinesis	Cdc15	S666	-2.87	0.001	F-BAR protein
	Cyk3	S300, S310	-2.24	0.03	Actin filament anchoring protein
	Rng10	T616, S632	-2.12	0.04	Coiled-coil protein
	Mid1	S328, S331	-1.84	0.01	Anillin-like medical ring protein

C

	Substrate	Site(s)	Ratio	Ratio (+)	p-value	Function
Septation	Sts5	S261, S264	-1.34	-1.20	0.04	RNA-binding protein
	Etd1	S51, S54	-1.25	-1.70	0.04	Spg1-binding protein

Figure 5

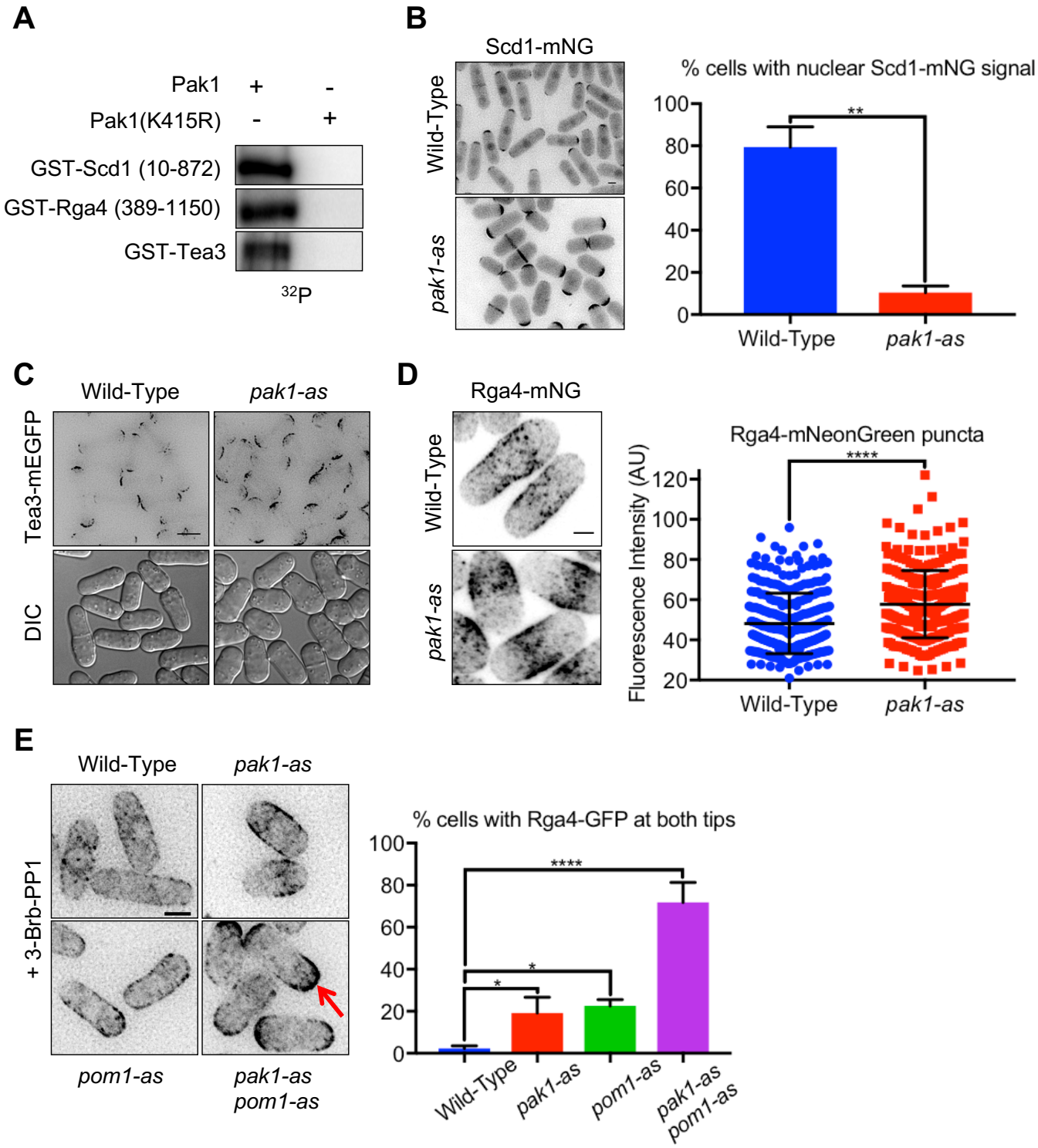
A
Pak1 + -
Pak1(K415R) - +
GST-Scd1 (10-872)
GST-Rga4 (389-1150)
GST-Tea3
32P
B
Scd1-mNG
Wild-Type
pak1-as
% cells with nuclear Scd1-mNG signal
100
80
60
40
20
0
**
Wild-Type
pak1-as
C
Wild-Type
pak1-as
Tea3-mEGFP
DIC
D
Rga4-mNG
Wild-Type
pak1-as
Rga4-mNeonGreen puncta
Fluorescence Intensity (AU)
120
100
80
60
40
20
****
Wild-Type
pak1-as
E
Wild-Type
pak1-as
+ 3-Brb-PP1
pom1-as
pak1-as
pom1-as
% cells with Rga4-GFP at both tips
100
80
60
40
20
0
****
*
*
Wild-Type
pak1-as
pom1-as
pak1-as
pom1-as

Figure 6

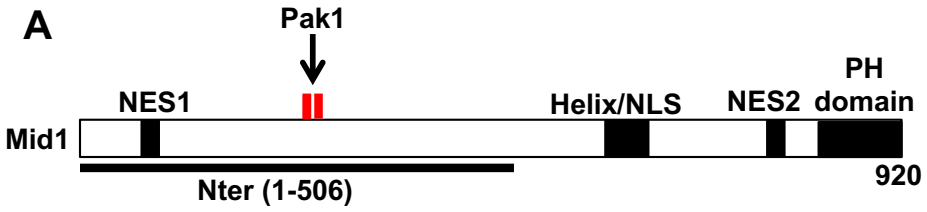
A
Pak1
NES1
Helix/NLS
NES2
PH domain
Mid1
920
Nter (1-506)

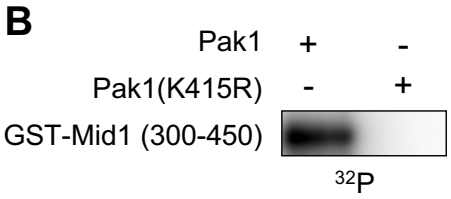
B
Pak1 + -
Pak1(K415R) - +
GST-Mid1 (300-450)
32P

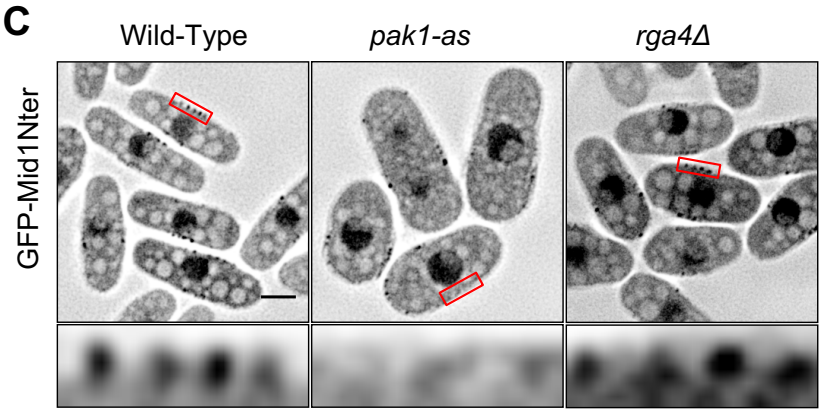
C
Wild-Type
pak1-as
rga4Δ
GFP-Mid1Nter

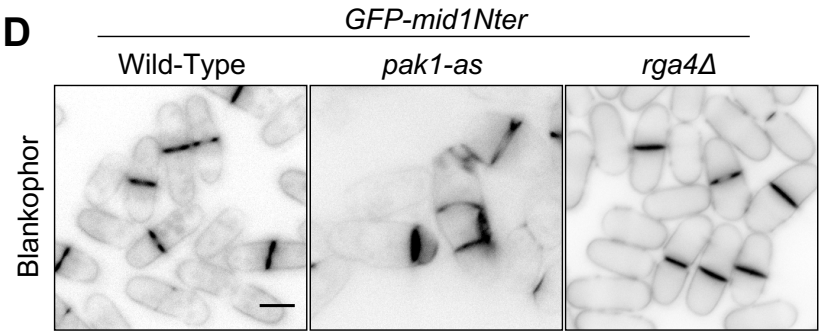
D
GFP-mid1Nter
Wild-Type
pak1-as
rga4Δ
Blankophor

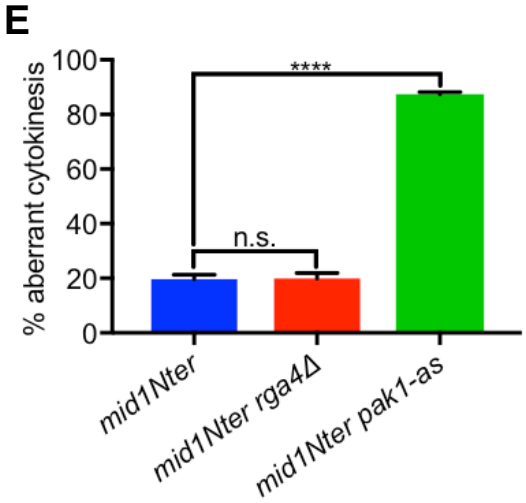
E
% aberrant cytokinesis
100
80
60
40
20
0
****
n.s.
mid1Nter
mid1Nter rga4Δ
mid1Nter pak1-as

Figure 7

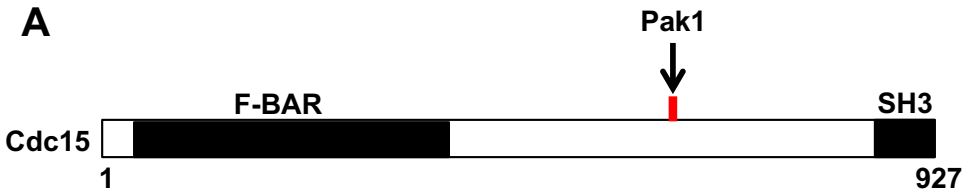
A
Pak1
F-BAR
SH3
Cdc15
1
927

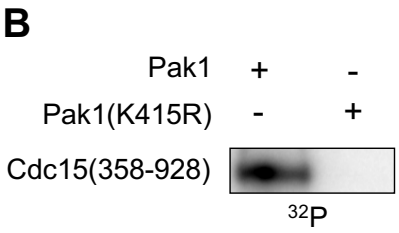
B
Pak1 + -
Pak1(K415R) - +
Cdc15(358-928)
32P

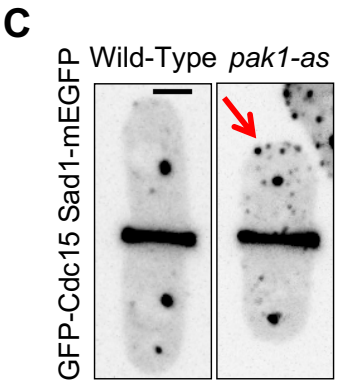
C
Wild-Type
pak1-as
GFP-Cdc15 Sad1-mEGFP

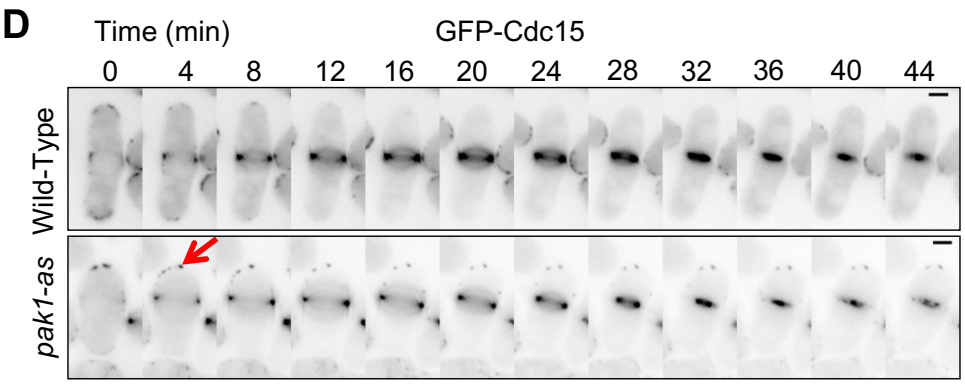
D
Time (min)
GFP-Cdc15
0 4 8 12 16 20 24 28 32 36 40 44
Wild-Type
pak1-as

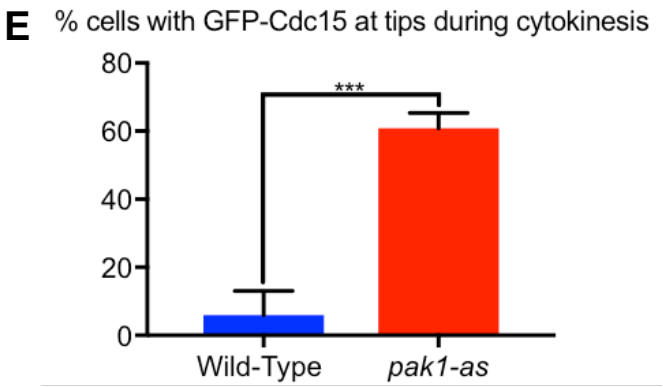
E
% cells with GFP-Cdc15 at tips during cytokinesis
80
60
40
20
0
***
Wild-Type
pak1-as

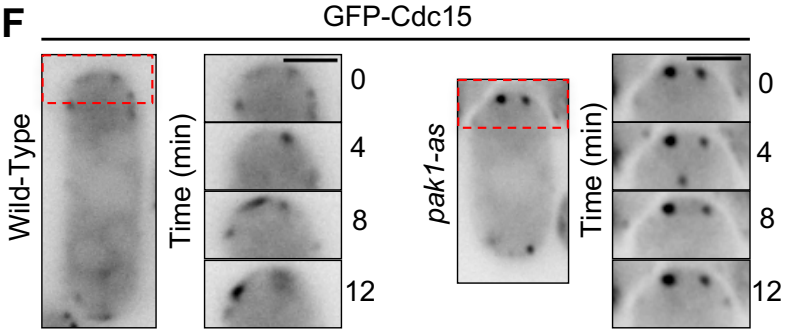
F
GFP-Cdc15
Wild-Type
Time (min)
0
4
8
12
pak1-as
Time (min)
0
4
8
12

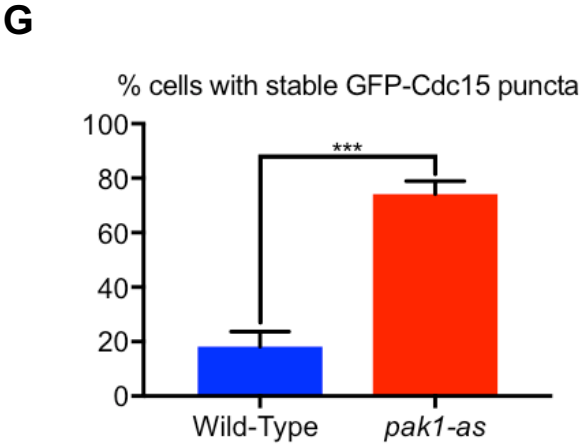
G
% cells with stable GFP-Cdc15 puncta
100
80
60
40
20
0
***
Wild-Type
pak1-as

Figure 8

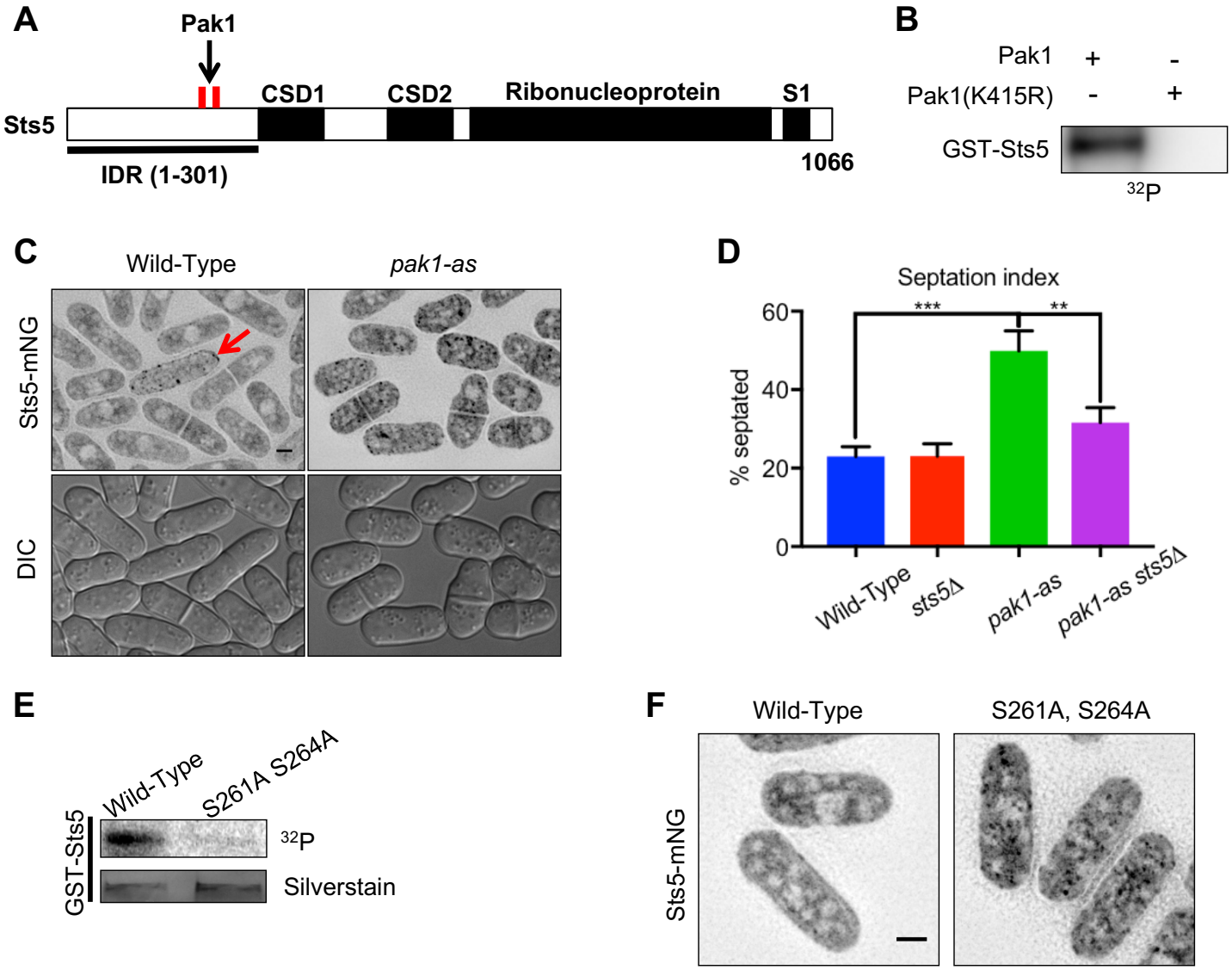
A
Pak1
CSD1
CSD2
Ribonucleoprotein
S1
Sts5
IDR (1-301)
1066
B
Pak1
+
-
Pak1(K415R)
-
+
GST-Sts5
32P
C
Wild-Type
pak1-as
Sts5-mNG
DIC
D
Septation index
% septated
60
40
20
0
***
**
Wild-Type
sts5Δ
pak1-as
pak1-as sts5Δ
E
Wild-Type
S261A S264A
GST-Sts5
32P
Silverstain
F
Wild-Type
S261A, S264A
Sts5-mNG

Figure 9

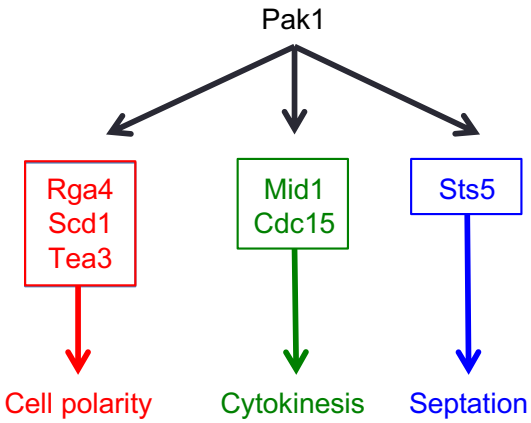
Pak1
Rga4
Scd1
Tea3
Mid1
Cdc15
Sts5
Cell polarity
Cytokinesis
Septation

Figure 10

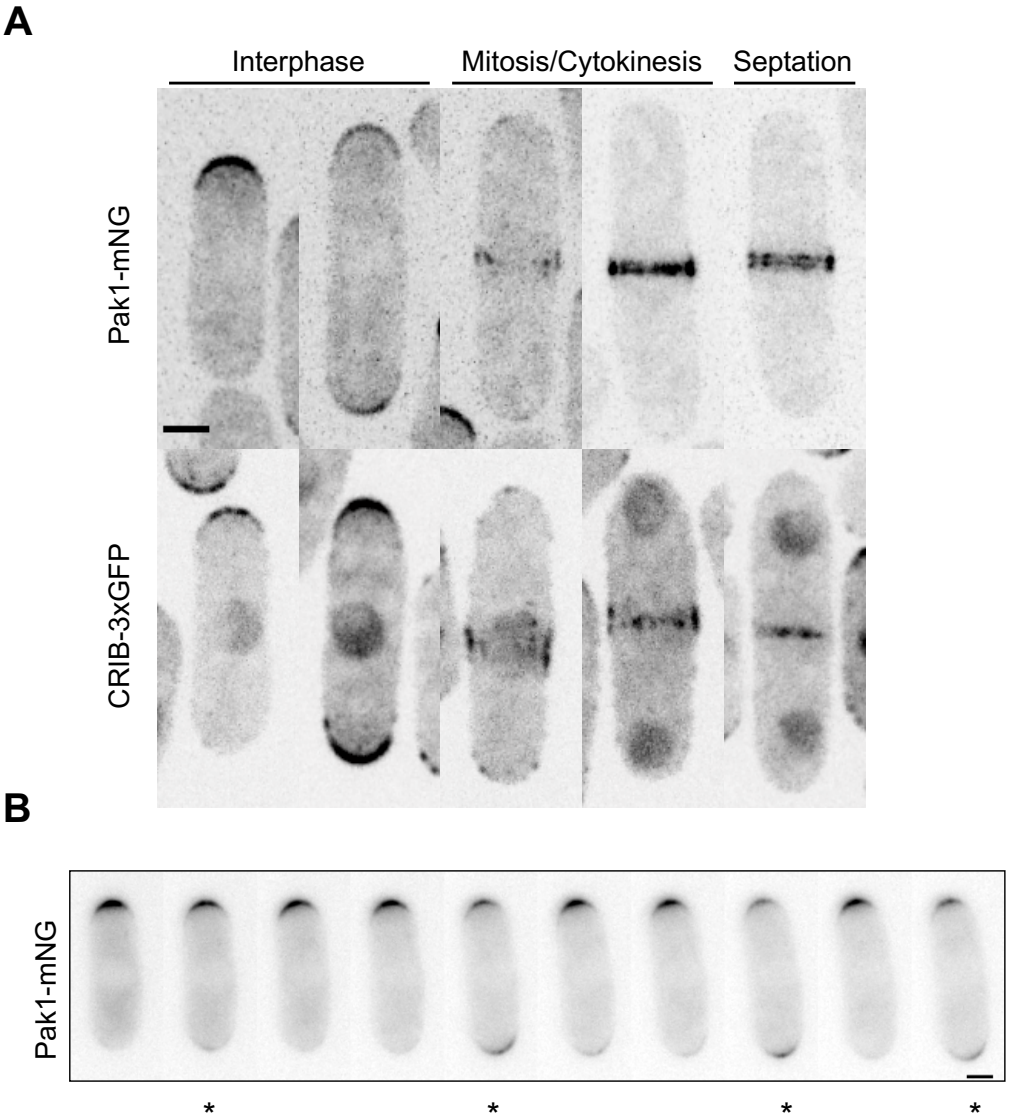

Supplemental Figure S1

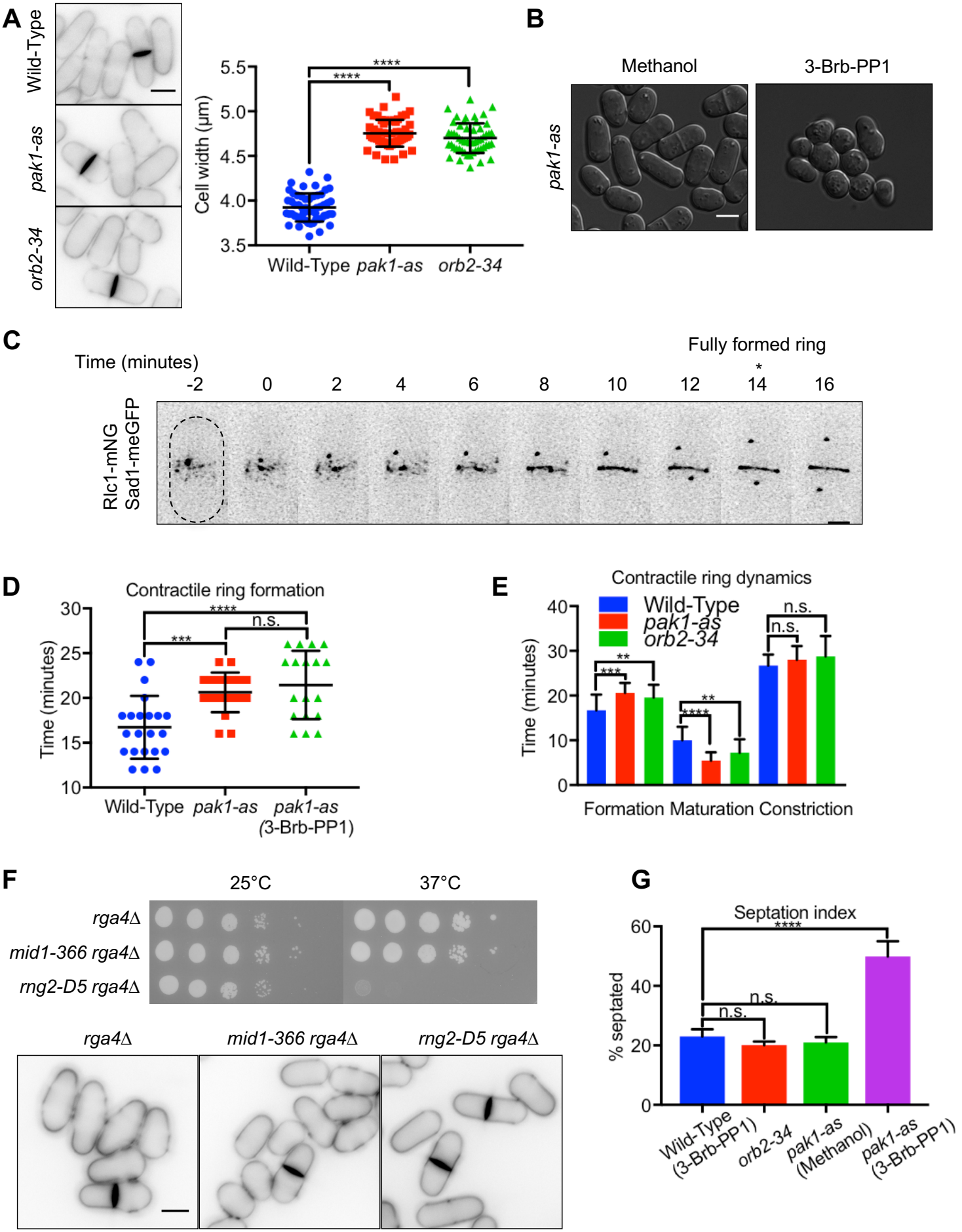

Supplemental Figure S2

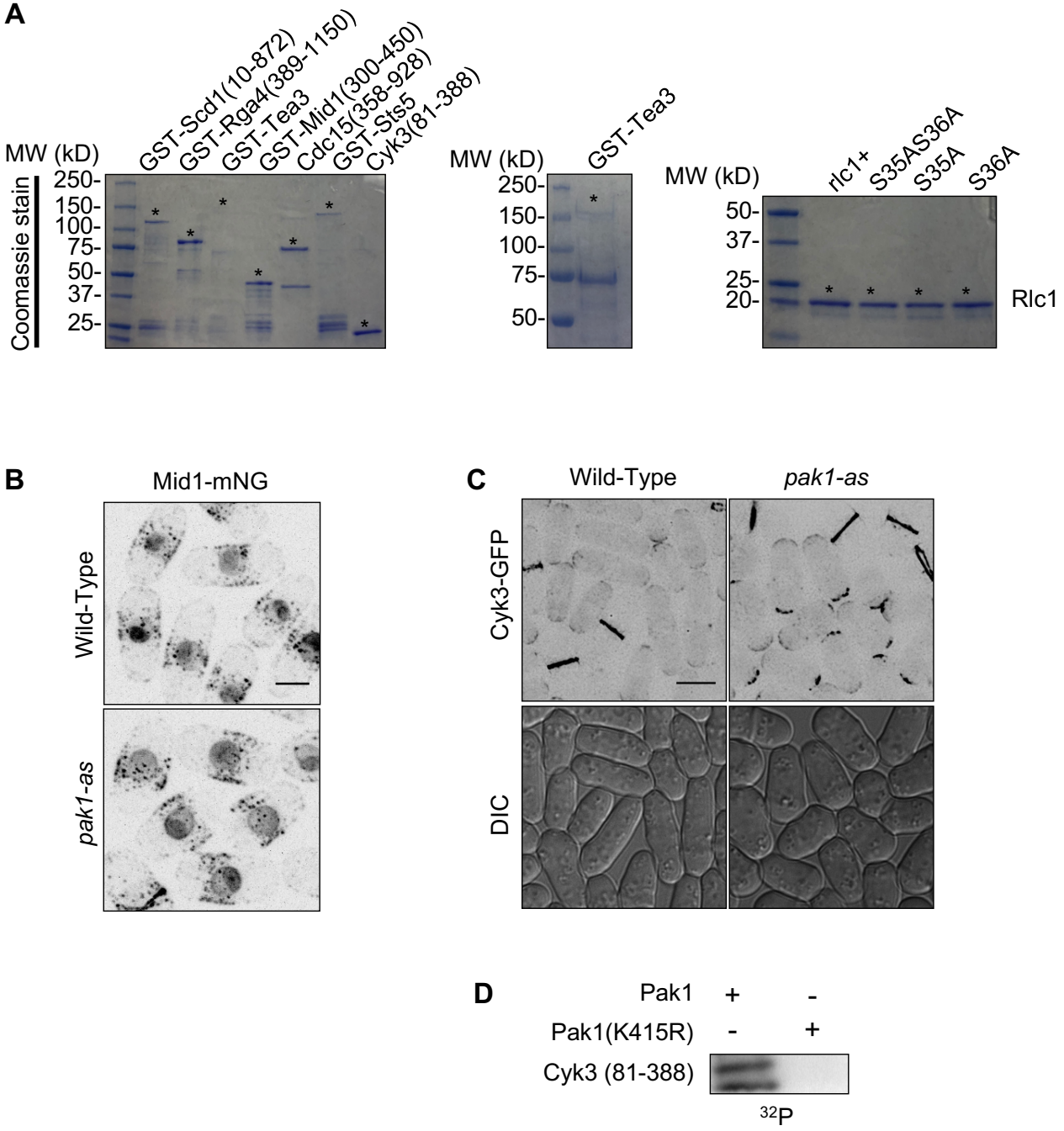

Supplemental Figure S3